Saturn's open-closed field line boundary: a Cassini electron survey at Saturn's magnetosphere

Jamie M. Jasinski[1,*], Christopher S. Arridge[2], Alexander Bader[2], Andrew Smith[3,4], Marianna Felici[5], Joe Kinrade[2], Andrew J. Coates[3,4], Geraint H. Jones[3,4], Tom Nordheim[1], Lin Gilbert[3,4], Abigail R. Azari[6], Sarah V. Badman[2], Gabrielle Provan[7], Nick Sergis[8] and Neil Murphy[1].

1. NASA Jet Propulsion Laboratory, California Institute of Technology, Pasadena, CA, USA.

2. Dept. of Physics, Lancaster University, Lancaster, UK.

3. Mullard Space Science Laboratory, UCL, Dorking, UK.

4. Center for Planetary Sciences at UCL/Birkbeck, London, UK.

5. Center for Space Physics, Boston University, Boston, MA, USA.

6. Dept. of Climate and Space Sciences and Engineering, University of Michigan, MI, USA.

7. Dept. of Physics and Astronomy, University of Leicester, UK.

8. Office for Space Research, Academy of Athens, Athens, Greece.

* Corresponding author: Jamie Jasinski (jasinski@jpl.nasa.gov)

Key Points:

- The high-latitude magnetosphere is predominantly in a state of constant plasma depletion and located on open field lines.
- The reconnection x-line is located at 20 – 25 R_S downtail from the planet on the midnight to dawn side of the equatorial magnetosphere.
- The open-closed field boundary is located at colatitudes of 12.7±0.6º and 14.5±0.6º (north and south) with weak PPO modulation in the north.

Abstract

We investigate the average configuration and structure of Saturn's magnetosphere in the nightside equatorial and high-latitude regions. Electron data from the Cassini Plasma Spectrometer's Electron Spectrometer (CAPS-ELS) is processed to produce a signal-to-noise ratio for the entire CAPS-ELS time of operation at Saturn's magnetosphere. We investigate where the signal-to-noise ratio falls below 1, to identify regions in the magnetosphere where there is a significant depletion in the electron content. In the nightside equatorial region we use this to find that the most planetward reconnection x-line location is at 20 – 25 R_S downtail from the planet in the midnight to dawn sector. We also find an equatorial dawn-dusk asymmetry at a radial distance of >20 R_S which may indicate the presence of plasma depleted flux tubes returning to the dayside after reconnection in the tail. Furthermore, we find that the high-latitude magnetosphere is predominantly in a state of constant plasma depletion and located on open field lines. We map the region of high-latitude magnetosphere that is depleted of electrons to the polar cap to estimate the size and open flux content within the polar caps. The mean open flux content for the northern and southern polar caps are found to be 25±5 and 32±5 GWb, respectively. The average location of the open-closed field boundary is found at invariant colatitudes of 12.7±0.6º and 14.5±0.6º. The northern boundary is modulated by planetary period oscillations more than the southern boundary.

1 Introduction

The Earth's magnetosphere is largely driven by its interaction with the solar wind [Dungey, 1961]. Saturn's magnetosphere is driven by internal processes as well as the external solar wind [e.g. Cowley & Bunce, 2003; Vasyliunas, 1983]. At the dayside magnetopause and the magnetotail, Dungey-type magnetic reconnection occurs to open and close magnetospheric flux, respectively. On the dayside this involves injecting plasma from the magnetosheath into the high latitude open magnetosphere and into the region known as the cusp [Jasinski et al., 2014, 2016a]. Both the northern and southern cusp have been measured at Saturn's magnetosphere [Arridge et al., 2016; Jasinski et al., 2017a]. On the nightside, Dungey-cycle magnetic reconnection drives open fields in the lobes to be closed, and during this process plasma is released down the tail

[e.g. Hill et al. 2008, Jackman et al., 2014, 2016; Smith et al., 2016, 2018a]. Therefore, the open magnetosphere is located at the polar regions where the field is tethered to only one of the polar ionospheres.

The process of reconnection at Saturn's magnetopause occurs under different conditions in comparison to magnetospheres located closer to the Sun such as Earth and Mercury [e.g. Masters, 2018]. The solar wind decreases in plasma density as a function of radial distance from the Sun, while the velocity remains constant. This causes the solar wind to increase in Alfvenic mach number with distance from the Sun, and therefore the shocks formed at the outer planetary magnetospheres produce a much higher plasma-β (ratio of plasma to magnetic pressure) in the magnetosheath. Such conditions have been shown to not be conducive for reconnection onset [Swisdak et al., 2003, 2010; Masters et al., 2012], in comparison to Earth and Mercury [e.g. Fu & Lee, 1984; Zhong et al., 2013; Slavin et al., 2012, 2014; Jasinski et al., 2017b]. Regardless, reconnection under such conditions at Saturn has been observed to occur at multiple x-lines to form flux transfer events [Jasinski et al., 2016b] similar to observations at the inner planets. Other evidence of reconnection has also been found at Saturn's magnetopause [e.g. Jasinski et al., 2014; Badman et al., 2013; Fuselier et al., 2014], as well as its effects in the aurora [e.g. Kinrade et al., 2017; Radioti et al., 2011, 2013; Palmaerts et al., 2016].

In contrast to external influences, the dynamics at Saturn's magnetosphere are largely driven internally [e.g. Vasyliunas 1983]. Interchange events occur and are thought to be due to a Rayleigh-Taylor like instability driven by centrifugal forces from Saturn's rapid rotation and the plasma loading from the icy moon Enceladus [Southwood & Kivelson, 1987; Thomsen et al., 2013, Achilleos et al., 2015; Rymer et al., 2009; Jones et al., 2006; Tokar et al., 2006]. The centrifugal forces exerted on the plasma also stretch the plasma sheet into a magnetodisk type configuration, which due to the impinging solar wind on the Saturnian magnetosphere, is bowl-shaped [Arridge et al., 2008a]. Centrifugal stresses cause the field to be stretched tailwards and magnetic reconnection occurs between closed field lines [Vasyliunas, 1983] – in contrast to Dungey-type reconnection, which occurs between two open lobe fields on the nightside. Recently, Vasyliunas-type reconnection has also been observed in the dayside Saturnian magnetodisk [Guo et al, 2018a,b].

The role of Dungey-type reconnection, even though less important as a driver of dynamics in the inner magnetosphere, shapes the outer structure and dynamics of the high latitude magnetosphere. Even though reconnection has been studied during various single event observations, the configuration of Saturn's global magnetosphere at any point in time is challenging to assess with a single spacecraft. Dungey-type magnetic reconnection on the dayside magnetopause fills the high latitude magnetosphere with open flux, where the plasma content will be lost along the open field. On the nightside, reconnection will release plasma down the tail. It is these areas that we investigate in this paper, and try to understand the average configuration of Saturn's magnetosphere.

In this paper we process the electron measurements from the Cassini Plasma Spectrometer's (CAPS) Electron Spectrometer (ELS). We investigate the locations where the magnetosphere is depleted of electrons below the instrument's detection threshold. Using all the ELS data available, we look at Saturn's magnetosphere as a whole, and investigate its average structure globally. We also investigate the data on an orbit-to-orbit basis to identify the open closed field line boundary (OCB).

In Section 2 we discuss the instrumentation and the method to reduce the ELS data. In Section 3 we explore various regions of the magnetosphere within the data and explore the implications of what is found. In Section 4 we summarize and discuss our results. In Section 5 we state our final conclusions.

2 Method: Electron Spectrometer data reduction and coordinate systems

2.1 The Cassini Plasma Spectrometer: Electron Spectrometer (ELS)

The Electron Spectrometer (ELS) is part of the Cassini Plasma Spectrometer (CAPS) [*Linder et al*., 1998; *Young et al*., 2004; Lewis et al., 2010]. ELS is a hemispherical top-hat electrostatic analyzer that measures electron flux as a function of energy-per-charge with an energy range of 0.58-28250 eV/q. Once the electrons pass through the electrostatic plates they strike microchannel plates (MCP), which cause a cascade of secondary electrons. These electrons are then collected by eight anodes, which are arranged in an arc formation (therefore the

direction of electron can also be registered). Each anode covers a field of view (FOV) of 20ºx5º, providing the instrument with an instantaneous FOV of 160º x 5º. Cassini is not a spin-stabilized spacecraft and CAPS is therefore mounted on an actuator to increase the angular coverage of the instrument, with a maximum actuation angle of ±104º at a rate of 1º s^{-1}. Therefore, the actuator and the ELS combined provide a coverage of 208º x 160º of spherical space which is approximately 56% of the full 4π space.

The potential across the analyzer plates is varied quasi-logarithmically (it is linear at low energies-per-charge) between 63 energy steps [Lewis et al., 2008]. ELS can perform a sweep across all energies for all anodes in 2s. The data is then packaged by the data processing unit, which averages the spectra according to the telemetry rate that is pre-selected. The data is usually averaged into 'A' and 'B' cycles. A-cycles contain 16 energy sweeps and so has a cadence of 32 seconds. B-cycles are made up of eight A-cycles: 256 s (more information about telemetry can be found in Table 1 of Arridge et al., 2009). For telemetry purposes, sometimes several sweeps are summed together resulting in lower time resolutions.

An example of a typical ELS spectrogram is shown in Figure 1a. Each of the 63 energy bins is shown (y-axis) with a range of fluxes. This data shows the data summed over all eight anodes during a high-latitude planetward trajectory through various regions in the local plasma environment.

The spacecraft can also become positively or negatively charged depending on the plasma environment that it is immersed in [Whipple, 1981]. In Figure 1a photoelectrons can be seen at energies lower than the ~10 eV spacecraft potential. For each bin in time the potential can be estimated by analyzing the energy spectra and locating the sharp decrease in counts near the ~0-40 eV level. The procedure for calculating the spacecraft potential specifically to ELS has been described and utilized in previous work [Johnstone et al., 1997; Lewis et al., 2008]. The spacecraft potential is shown in Figure 1a as the black line. In the analysis of this dataset we do not use times when the spacecraft potential was found to be negative. We also do not use any data from energy bins below the spacecraft potential. To account for any error in the spacecraft potential estimate we also do not use the first four energy bins above the estimated spacecraft

potential (four was chosen arbitrarily). The used potential (Figure 1a) can be seen to account for some photoelectrons at energies above the spacecraft potential in the polar cap. In the following sections we describe how we take the ELS data and reduce it to produce a signal-to-noise ratio (Figure 1b) for the entire ELS dataset, which is used for analysis. CAPS was switched off on June 1 2012 to safeguard the whole spacecraft after it emerged that there was a short circuit. Therefore, analysis of this dataset is only for 2004-2012.

2.2 Producing an omnidirectional electron flux and a signal-to-noise ratio

First, we calculate the uncertainties for the data at all anodes and all energy bins. During this process we average data over two A-cycles where possible and if A-cycles are not the lowest resolution available, we use the next available resolution (B-cycle). We average over two A-cycles to improve our counting statistics [e.g. Paschmann et al., 2000].

We calculate the uncertainties on the count rates (ε_{CR}) using counting statistics using $\varepsilon_{CR}=\sqrt{(\text{count rate/accumulation time})}$. The uncertainties are calculated for each anode and energy bin, and weighted accordingly depending on the averaging mode of the instrument. The uncertainties will minimize at five percent due to compression noise (due to the compression by the CAPS data processing unit, see Arridge et al., 2009 for more details), so the minimum uncertainty is set to five percent of the data count rate. We also estimate the ELS background and background uncertainty for each anode at its actuator angle. Data from ELS is contaminated with a count rate due to the radiation sources onboard Cassini. We use the method presented and described by Arridge et al., (2009) to estimate the model background as well as the uncertainty on the background. We subtract the background from the data to calculate the data signal and also propagate the background uncertainty so that the uncertainty (ε) is $\varepsilon=\sqrt{(\varepsilon_{CR}^2 + \varepsilon_{background}^2)}$.

Next, we produce a pitch angle distribution from the directional data available from the actuation of ELS and each of the 8 anodes using magnetometer (MAG) data [Dougherty et al., 2004]. We average the data into nine bins each covering 20º in pitch angle, where the first bin covers 0-20º, the fifth bin covers 80-100º, and the ninth bin covers 160-180º in pitch angle. We weight the averaging according to the area of the anode's FOV at that particular pitch angle direction. We

do not use data if an anode (for its actuation angle) is obscured by the spacecraft. For details about the obscuration of ELS FOV by Cassini itself, please see Lewis et al., (2008). To estimate the omnidirectional flux, we average over the pitch angle measurements and uncertainties. Finally, we average over all energies to create one bin and we obtain an omnidirectional signal-to-noise ratio (SNR) by dividing this data by its propagated uncertainty.

The final SNR can be seen in Figure 1b. The SNR can be seen to match the observations. At low fluxes in the high-latitude magnetosphere the SNR is 2-15, except for the intermittent drop to background plasma levels, whereby the SNR drops to 1 or below. When the spacecraft crossed into the cusp, fluxes increased and the SNR increased to ~30. Upon entering the region of magnetic field lines threading the polar cap, background fluxes of plasma were only detected, and the SNR was <1 and close to zero. Upon reentering the magnetosphere, fluxes (SNR >1) increased until the spacecraft entered the region of penetrating radiation towards the end of the timeseries. Therefore, the SNR is a good parameter to differentiate between times (and regions) when ELS observed high electron fluxes (i.e. above background fluxes), and when the electron fluxes were at background levels (and so CAPS did not measure magnetospheric electrons).

2.3 Removing data – Gains tests, and magnetosheath, solar wind and moon encounters

Degradation of the MCP over time meant CAPS would have repeated tests throughout the mission to check the gains loss (to vary the voltage to recover the loss). This engineering mode was scheduled to occur approximately every 50 days [Young et al., 2004]. In total there were 151 days of gains tests throughout the mission (available in the online supporting material), where the data is unreliable and therefore has been removed from this study.

Since the interest of this investigation is to analyze Saturn's magnetosphere, we have removed excursions outside of the magnetopause. Data from multiple boundary crossings is not used so that we do not capture any boundary processes. Therefore, all data was removed from within a time frame from the first outbound magnetopause crossing until the last inbound crossing for each orbit. This list of crossings is provided in the online supporting material. Flybys of the major Saturnian moons were also removed including Titan, Rhea, Enceladus, Tethys, Dione, Iapetus and Hyperion. Data within a distance of 10 moon radii was removed [e.g. Roussos et al., 2012; Krupp et al., 2013]. In total, 38% of the data was removed due to spacecraft excursions

into the magnetosheath and solar wind, while 9% of the data was removed due to gains tests and moon encounters.

2.4 Coordinate systems

The position of Cassini is shown here in Kronocentric Solar Magnetic (KSMAG) coordinates. KSMAG is a Saturn centered coordinate system, where **Z** points along the dipole moment **M**, **Y**=**M**×**S** (in the duskward direction) where **S** is the vector pointing from Saturn to the Sun. **X** completes the right-handed set and is in the **M**-**S** plane (Saturn-Sun and dipole plane). Due to the alignment of the magnetic dipole with the spin axis to within less than 0.01º [Dougherty et al., 2018], Z also points along the spin axis. This means that the current sheet is along the dipole equator during the different Saturnian seasons meaning it is always anchored in the X-Y plane (Cassini was at Saturn during southern summer and equinox during CAPS operation from 2004-2012, equinox was in August 2009). The various coordinate systems used during the Cassini mission are described by Arridge et al., (2011a).

2.5 Estimating where plasma depletion is observed in Saturn's magnetosphere

From the calculated SNR we have produced maps of the magnetosphere in various regions and planes and binned the data in location (1 R_S^2 bins), specifically in regards to where Cassini measured plasma above background levels (SNR > 1) and where it did not (SNR ≤ 1). To calculate how often in a region of space Cassini observed no plasma (i.e. no measured electron flux above the background) we first calculated the fraction of ELS data below the background for each Cassini orbit (to have visited that 1 R_S^2 bin) and then averaged over all orbits. This results in a color bar from white to red (see Figure 2). White shows that everytime Cassini explored that bin it always detected plasma above the background for every accumulation in every orbit. Dark red (end of the color scale) shows that everytime that Cassini was in that bin it never observed plasma above background detection levels (grey represents no data). For some locations (such as in the deep tail) where Cassini has only had one orbit in a particular bin, this results in an average over 1 orbit (rather than an average of a few orbit averages). This color scheme is unconventional (traditionally light colors usually represent low values or fluxes and dark colors represent high values) however it is the best color scheme to show the stark contrast

from where flux tubes are measured with a low plasma content (red) in comparison to where high plasma fluxes and densities are observed (white).

3 Results

3.1 Equatorial plane - Tail reconnection x-line

Figure 2 shows the results from the above data analysis method in the X-Y plane. The data shown in Figure 2 is from within 5º latitude and 2.5 R_S of the dipole equator. A model magnetopause (Kanani et al., 2010) is shown with a standoff distance of approximately ~27 R_S, which is the upper value from the bimodal distribution (lower value ~22R_S) of the magnetopause location found by Achilleos et al., (2008). Titan's orbit (20 R_S) is also shown.

Individual orbits, which had very high altitudes at apoapse, can distinctly be seen in the plot (in the deep magnetotail at X_{KSMAG}~70 R_S). Generally, it can be seen that within 20 R_S, the magnetosphere possesses a high plasma content and this is the region that is largely driven by plasma interchange events (< 15 R_S). Interchange events have been well investigated during the Cassini era and were observed by a variety of instruments [e.g. Azari et al., 2018, 2019; Andre et al., 2007; Burch et al., 2005; Thomsen et al., 2014; Paranicas et al., 2016; Lai et al., 2016; Kennelly et al., 2013].

As Cassini travels further away from Saturn it enters a different dynamical regime, where processes in the tail dominate the plasma and magnetic structure of the magnetosphere. Tail reconnection takes place in the tail from either Vasyliunas or Dungey-type magnetic reconnection as mentioned above. Through these processes, plasma is lost from the system and escapes downtail. From ~20 R_S outwards, on the night and dawnward sides in local time, most of the ELS observations suggest that the flux tubes are plasma depleted (plasma is lost downtail after magnetic reconnection).

To explore this further, we present the data in the warped current sheet reference frame. Arridge et al., (2008a) showed that the plasma sheet residing in the magnetodisk is 'bowl' shaped due to the solar wind impingement being transmitted to the disk and causing the current sheet to be moved out of the rotational or dipole equator. Therefore, the data shown in Figure 2 could just be

of the lobes as the spacecraft could be outside the current sheet. The model current sheet distance from the equator z_{CS} in the KSMAG coordinate system is:

$$\boldsymbol{z_{CS} = \left[r - R_H \tanh\left(\frac{r}{R_H}\right)\right] \tanh \theta_{SUN}} \quad (1)$$

where r is the cylindrical radial distance, R_H is the hinging distance and equal to 29 R_S and $\boldsymbol{\theta_{SUN}}$ is the solar wind latitude [Arridge et al., 2008; Carbary et al., 2019]. Figure 3a shows the ELS data within 2.5 R_S of the warped model current sheet. The current half-sheet thickness has previously been found to range between 2 R_S and 4 R_S [e.g. Connerney et al., 1983; Giampieri and Dougherty, 2004], with more recent investigations estimating thicknesses of 1.5 - 2.5 R_S [Arridge et al., 2008b; Kellet et al., 2009, 2011; Carbary et al., 2012; Sergis et al., 2009, 2011] while Martin et al., (2017) found values of 2-6 R_S. Therefore, our use of a current sheet half-thickness of 2.5 R_S is reasonable.

Comparing Figure 2 to 3a, it can be seen that a large portion of the deep tail orbits were outside of the warped current sheet. The 'x' shows the location of reconnection signatures [Smith et al., 2016] that were observed by Cassini during the same times as the ELS data displayed (detection of plasmoids and dipolarizations). Dipolarization signatures occur after magnetic reconnection in the magnetotail, where the planetward magnetic field relaxes and becomes more dipolar [Slavin et al., 2002; Bunce et al., 2005]. Plasmoids and dipolarizations have both been investigated at Saturn [e.g. Hill et al., 2008; Thomsen et al., 2013; Jackman et al., 2014; Smith et al., 2018a], and are also commonly observed at the magnetospheres of Mercury [e.g. Dewey et al., 2017] and Earth [e.g. Hones et al., 1976; Ieda et al., 1998; Arnold et al., 2018].

Figure 3a shows the boundary between where high and low fluxes of plasma are observed in the night side tail, at approximately 20-25 R_S radial distance. Figure 3a presents a statistical average of where the planetward most boundary between flux tubes with low and high plasma content is located and therefore shows where the most planetward reconnection x-line is located at Saturn. It is also notable that in a plasma system with so much variability, the location of this boundary is consistently observed on a number of orbits spread in local time. This is supported by the locations where Cassini observed reconnection signatures, which also lie largely on the portion

of orbits where ELS detected little or no electrons. This is consistent with MHD modeling of Saturn's magnetosphere [Jia et al., 2012] that presented the x-line to be located at X~ -25 R_S downtail at midnight local time, which then retreated to X~ -30 R_S downtail by the end of the simulation. Our observational average is similar to in situ observations of reconnection in the tail (at 01:30UT) at a radial distance of ~29 R_S [Arridge et al., 2016b]. In comparison to Jupiter, the x-line in the Jovian magnetosphere has been found to be located at ~90 R_J [Vogt et al., 2012, 2014].

3.2 Equatorial plane - Local time asymmetry

Figure 3b shows the same dataset from 3a, but in local time [LT] – [R] radial distance. The boundary between flux tubes with high and low plasma content can be observed to continue into the dawn and morning dayside sector of the magnetosphere, showing a local time asymmetry between the morning and afternoon sectors. A dawn-dusk asymmetry has also been observed in the thermal ion population [Felici et al., 2018]. We suggest that this is evidence of the return flow of plasma depleted flux tubes from the nightside to the dayside, similar to what is observed at Jupiter. At Jupiter there exists a "cushion region" which is caused by the rotation of depleted flux tubes into the dayside Jovian magnetosphere from dawn into the late morning [e.g. Smith et al., 1974, 1976; Balogh et al., 1992; Kivelson et al., 1997; Kivelson & Southwood, 2005]. This region also exhibits dipolar configurations of the magnetospheric field and magnetic nulls which arise from instabilities that form at the outer edge of the plasma sheet. Most recently there is evidence that the concept of the cushion region may need to be reassessed because the Juno spacecraft did not observe a persistent cushion region on the dawn flank [Gershman et al., 2018]. Went et al., (2011) compared observations from Jupiter (with the Ulysses spacecraft) and Saturn (Cassini) and concluded that Saturn lacked a cushion region of quasi-dipolar flux tubes. However, the authors conclude that evidence from more plasma data is needed to make a more conclusive statement.

From Figure 3b we propose that a cushion region in the form of depleted flux tubes at Saturn may exist, but it may not be entirely similar or exhibit exactly the same physical characteristics as that observed at Jupiter. A dawn-dusk asymmetry has also been found in the energetic plasma where the ring current becomes increasingly pressure gradient driven at dawn [Sergis et al.,

2017]. Therefore the return flow of depleted electrons at dawn found in this study may carry energetic plasma not observable by ELS. Further effort and investigations are required to make a more conclusive statement on this topic at Saturn (and it seems, also at Jupiter: Gershman et al., 2018).

3.3 High-latitude and polar observations

Figure 4 shows the ELS results in the X-Z plane (view from dawn) with the Sun to the right. This plot was made from the data during the high-latitude orbits from July 22 2006 until October 12 2009. The plasma depleted regions of the high latitude polar magnetosphere (red) can clearly be seen in stark contrast to the lower latitude regions with a high electron content. The nightside (at radial distances greater than ~10 R_S) contains much more variability at the boundary between the equatorial region and the lobes, and this is most likely due to the periodic oscillation or "flapping" of the current sheet, whereby the spacecraft repeatedly moves from the lobes into the current sheet on a single orbit [e.g. Arridge et al., 2009, 2011b; Sorba et al., 2018].

The dayside high latitude profile however is more coherent. There is a clear boundary between the two plasma regimes, which identifies the boundary between magnetospheric field lines that are open to the solar wind (magnetic field is tethered to the ionosphere in one hemisphere) and fields that are closed (both footpoints of the magnetic field are tethered to the ionosphere), otherwise known as the open-closed boundary (OCB). This boundary contains Saturn's magnetospheric cusp [Jasinski et al., 2014, 2016a, 2017; Arridge et al., 2016a].

Figure 4b shows the latitudinal distribution of electrons on the dayside with radial distance. The OCB can clearly be seen decreasing in latitude with increasing radial distance (at the boundary between high and low electron signal). This boundary is also more equatorward in the south than in the north. The difference between the northern and southern hemispheres is most likely attributed to the fact that our observations are not centered on equinox (August 2009) and so for most of these observations the Sun was tilted below the equator to the south (similarly found at Earth, Wing et al., 2005). The equatorial plasma is forced northwards due to the warping of the current sheet [Arridge et al., 2008a], which acts to push the location of the northern OCB (and

cusp) polewards. The location of the cusp and the OCB is also at much lower latitudes in the northern mid-altitude region (~45º at 15 R_S) than that observed at Earth (~75º, Zhou & Russell, 1997). This is most likely due to massive departure from a dipolar configuration with the radial extension of the field lines on the dayside magnetosphere (in comparison to Earth). In the next section we explore this high latitude OCB further.

3.4 Open flux estimates - Mapping ELS data to the polar ionosphere

The data is mapped to the ionosphere using an axisymmetric magnetic field model with a superimposed model ring current field. The axisymmetric internal magnetic field is calculated as a spherical expansion and uses the coefficients from Burton et al., (2010), where g^0_1, $g^0_{2, \text{ and }} g^0_3$ are the Gauss coefficients taken to be 21136, 1526 and 2219 nT, respectively. The model ring current field parameters are taken from Bunce et al., (2007) and the model is also dependent on the magnetopause standoff distance. Here we have taken the standoff distance as 24.5 R_S, which is the mid-point between the two values (22 and 27 R_S) of the bimodal distribution of the average Saturn magnetopause location [Achilleos et al., 2008]. Changing the standoff distance does not vary the invariant colatitude significantly (the colatitude of the magnetic field line at 1 R_S). As an example, the invariant colatitude for the cusp observation on January 21 2009 (19:00 UT) [Jasinski et al., 2014] estimated with a standoff distance of 24.5 R_S is 8.7º whilst for a standoff distance of 22 and 27 R_S the colatitude is 8.6 and 8.8º, respectively. The field vectors associated with the ring current sheet are calculated from the model described by Connerney et al., (1981, 1983), using the analytical approximations presented by Giampieri and Dougherty (2004). This model has previously been used to analyse high-latitude cusp observations [Jasinski et al., 2017a] as well as map the footpoint of the magnetic field [e.g. Jinks et al., 2014]. The data from each hemisphere of the magnetosphere is mapped to its polar ionosphere.

The results are shown in Figure 5a) for the northern and b) the southern hemispheres. The data is binned in 5º local time longitude bins (~20 minutes in LT) and 2º colatitude bins. Firstly, it can be seen that Cassini did not explore all the mapped regions of the polar magnetosphere. There are orbital biases towards dusk (for the north) and dawn (for the south). The average statistical location of the center (black) of the UV auroral oval and its poleward and equatorward edges

(grey) from Bader et al., (2019a) are also shown. The OCB is expected to be observed just poleward of the auroral oval [e.g. Cowley et al., 2003, 2005; Bunce et al., 2008; Jinks et al., 2014]. The high latitude polar magnetospheric areas with plasma depleted flux (red) are expected to be on open fields.

Therefore Figure 5 is a good statistical representation of the open (red) and closed (white) field line boundary. From this we try to estimate the average amount of open flux at Saturn. First, we identify the outer edge of the OCB by selecting the largest difference in plasma content between bins in longitude. Where there is no data we take the average OCB colatitude (this is calculated below in Section 3.5) of 12.7º for the north and 14.5º for the south. Using the coefficients from Burton et al., (2010), mentioned above, we employ the method used by Badman et al., (2005, 2014) who calculated open flux estimates from auroral observations using a flux function F(R, θ). We integrate over the polar cap area to calculate the amount of open flux, Φ:

$$\boldsymbol{\Phi = \Delta\phi \sum_{n=1}^{72} F(R(\theta_n), \theta_n)} \qquad \textbf{(2)}$$

where Δϕ is the width in local time longitude (and equal to 5º), the colatitude for a longitude sector *n* is θ_n, and $R(\theta_n)$ is the radius of polar cap at that longitude. Please see Badman et al., (2005) for a detailed description of this method.

We calculate open flux estimates for the north and south to be 25±5 and 32±5 GWb, respectively. The errors are estimated from the half-width of the latitudinal bins shown in Figure 5. These values fall within the range of 10-50 GWb estimated by Badman et al., (2014), however they represent a more average representation of the open flux estimated at Saturn.

3.5 The OCB and planetary period oscillation (PPO)

Figure 6 shows the observations for an individual northern polar cap crossing. These observations are during Rev-99. Figure 6a, shows the mapped trajectory of Cassini (red) in the northern hemisphere. The observed OCB location is show by the blue star. Figure 6b shows auroral observations by UVIS on the same day, the mapped location of Cassini during these auroral observations (yellow diamond) is shown. Figure 6c-d show Cassini's radial distance from Saturn, and latitude. Figure 6e-f presents the SNR and a full electron spectrogram measured by ELS for this time period, respectively. Whilst crossing field lines that are open and connected to

Saturn's polar cap the SNR is continuously close to zero, and only background electron fluxes are observed. Upon crossing the OCB onto closed field lines there is an abrupt increase in the SNR to values >1. It is at this location that the OCB is selected and shown as dashed vertical lines (for the north and south). For the northern OCB, the mapped location is shown as a blue star in Figure 6a and b. The invariant colatitude (Λ) of the OCB for all the orbits where it is possible to detect is shown in Figure 7a and 7b (for each Rev) and also for local time in 7c-d. While there is typically good agreement between ELS detecting background level of plasma and the identification of open fields, it should be noted that this agreement is not universal. As shown by Jinks et al., (2014), the difference in latitude of the identified OCB by ELS is on average 0.34º different than that identified by the measurement of energetic electrons by the Magnetospheric-Meaurement-System (MIMI).

Using the OCB location measured from each individual orbit, the OCB has a mean invariant colatitude value of 12.7±0.6º and 14.5+0.6º for the north and south, respectively. The errors are calculated from 1) the variation of the colatitude mapping dependent on the magnetopause location from the magnetic field model (mentioned above) and 2) the mean difference in OCB location found between our results and those estimated by Jinks et al., (2014) (discussed further below). In comparison to the OCB investigation by Jinks et al., (2014) our values are lower (north: 13.3º, and for the south: 15.6º). However, we have analysed more orbits than the Jinks et al., (2014) study, which only included up to Cassini's Rev-96 and 100 for the north and south respectively. They only analyzed the OCB for a total of 48 crossings (22 in the north and 26 in the south) whilst our dataset contains 86 crossings (44 in the north and 42 in the south). The primary difference between the Jinks et al. (2014), study and ours is that we investigate the OCB with ELS data whilst they do so with three seperate datasets (RPWS, ELS and MIMI-LEMMS). Their investigation relies on observations from all three of these datasets, however, we are not restricted by the other instruments to complete our analysis for as many orbits as possible. Of the orbits that Jinks et al., (2014) identified the OCB in the ELS dataset, the mean difference in invariant colatitude between their values and ours are ~0.5 and 0.4º for the north and south, respectively, with medians of ~0.3 and 0.2º. Therefore, both methods estimate similar values.

We have also inspected the data of the OCB for any modulation by the planetary period oscillation (PPO) systems. PPOs are observed in the plasma and magnetic field data at a period

close to the planetary rotation period [e.g. Carbary & Mitchell, 2013] and can be best modelled as two rotating magnetic perturbation fields (one in the north and one in the south) that rotate independently of each other and are associated with field aligned currents that perturb the local plasma environment [e.g. Andrews et al., 2010, 2012; Hunt, et al., 2014, 2015, 2016; Provan et al., 2011, 2015, 2016, 2018; Bader et al., 2018, 2019b]. Many magnetospheric processes and boundaries are modulated by the PPO systems [e.g. Clarke et al., 2010; Jackman et al., 2016; Badman et al., 2012; Paranicas et al., 2005; Bradley et al., 2018; Carbary, 2017].

The local time longitude (ϕ) must be converted to a PPO longitude $\Psi_{N/S}=\phi_{N/S}(t)-\phi$, for both the northern and southern PPOs, where $\phi_{N/S}(t)$ is the phase angle describing the instantaneous orientation of the PPO magnetic perturbation fields with time (for the separate northern and southern systems). The phase angle for the whole Cassini mission is estimated by Provan et al., (2016) and provided by the authors on their university website (link in acknowledgements). The phase positions are shown for the observations in Figure 6b.

To complete this we have taken a small bin (10º wide, near the peak of number of observations) in local time for each hemisphere; 5º within a LT-longitude of 0º (local midnight) in the south and 5º within a LT longitude of 320º (pre-midnight), in the north. By selecting a narrow local time bin we avoid any variation of the invariant colatitude (Λ) that may occur in local time that is independent of the PPO modulation. These local time longitudes are then converted to PPO longitude for the north and south ($\Psi_{N/S}$), for each hemisphere. Each hemisphere may be affected by the PPO system in that hemisphere (the primary PPO system) as well as the opposite hemisphere (secondary PPO system). The displacement from the mean invariant colatitude against the PPO longitude is shown in Figure 7e-h. The modulation is fitted with cosine functions similar to previous investigations of the auroral modulation by PPO's [Bader et al., 2019a; Nichols et al., 2008; 2016]. We find the best-fit cosine functions by minimizing χ^2 (both the function and minimized χ^2 are shown on the plot). The lower χ^2 for the northern hemisphere shows that the northern OCB is modulated by PPOs more than the southern OCB. This is in contrast to Jinks et al., (2014) who found the southern OCB to be more organized by PPOs (than the northern OCB). Our method however takes a very narrow bin in local time, and therefore is more reliable (the authors used all their observations, which will introduce an uncertainty if the

OCB is not a perfect circle). For the northern OCB, the negative displacement peak at Ψ_N=175º is very similar to the auroral oval displacement peak found Ψ_N ~165º [Bader et al., 2019a].

4 Summary and Discussion.

In this paper we have processed and analyzed data from the Electron Spectrometer (ELS) onboard Cassini in regards to a variety of phenomena at Saturn's magnetosphere. The data from ELS (2004-2012) had photoelectrons below the spacecraft potential removed as well as background levels of electron flux subtracted. The computed flux and its uncertainty were then binned to produce a timeseries of the electron signal-to-noise ratio (SNR) for the entire dataset during the first 8 years of the Cassini mission. After removing data during inflight engineering tests of the instrument, excursions into the magnetosheath and solar wind, as well as moon flybys, the dataset was analysed in regards to where the electron SNR falls to background levels in Saturn's magnetosphere (SNR $\leq$ 1).

Firstly, the nightside equatorial magnetosphere was investigated by transforming the dataset into the equatorial warped current sheet plane. It was found that on the post-midnight to dawn region the electron content in the magnetosphere falls to background levels. The nightside region depleted of electrons is most likely caused by reconnection in the nightside where plasma is lost downtail. The reconnection x-line in the nightside was estimated to be located at a radial distance of 20-25 R_S in the midnight-dawn local time magnetosphere. This was compared to reported remote detection of reconnection signatures such as plasmoids and dipolarizations [Smith et al., 2018a], and is consistent with their values of the reconnection x-line occurring at 20-30 R_S downtail. Our estimated values are also similar to the MHD simulation of Saturn's magnetosphere [Jia et al., 2012], which found the reconnection x-line to be 25-30 R_S downtail at local midnight. However, it is important to remember that reconnection in MHD simulations occurs due to numerical diffusion (due to discretization of the MHD equations). This is not a realistic characterization of reconnection and leads to a larger reconnection rate and does not heat the plasma as much as a fully kinetic simulation. Nevertheless, MHD is useful at highlighting the possible topology of the magnetic field and it is encouraging to see the various estimations of the reconnection x-line to overlap significantly.

The results also showed a dawn-dusk asymmetry in the electron content of Saturn's magnetosphere. Similarly, a survey of the thermal ions in Saturn's magnetosphere also detected a dawn dusk symmetry [Felici et al., 2018]. These observations are not due to a noon-midnight electric field that has been measured at Saturn [e.g. Thomsen et al., 2012; Wilson et al., 2013; Andriopoulou et al., 2012, 2014]. This electric field results in a planetward movement of the plasma in the postnoon sector [Jia & Kivelson, 2016], which is not what we measure here. We observed a depletion of plasma continue into the morning region, most likely due to return flow of plasma depleted flux tubes. At Jupiter such a region has been called the cushion region and is accompanied by magnetic null regions and instabilities that form on the outer edge of the current sheet. These magnetic signatures have not been observed at Saturn [Went et al., 2011], and so it was concluded that the cushion region does not exist at Saturn. However our evidence of a local time asymmetry may indicate that this region of plasma depletion may occur at Saturn's magnetosphere. Further exploration of the plasma observations is required to make a more definitive conclusion. Dipolarization signatures of Dungey-style reconnection have also found density depleted flux tubes in the post-midnight region [Smith et al., 2018a,b]. Our conclusion that this phenomenon needs to be examined more closely is similar to a recent study of Juno spacecraft data by Gershman et al., (2018), that found that the concept of a cushion region at Jupiter also needs to be reassessed.

The high-latitude ELS measurements during the highly inclined orbits of Cassini in 2006-2009 were also analyzed. The results show that much of Saturn's high-latitude magnetosphere is depleted of plasma (Figure 4a). The latitudinal boundary at higher altitudes (> 10 R_S) between where plasma is and is not measured by ELS is much more well defined on the dayside, than in the nightside, which is most likely caused by the flapping of the magnetotail. The warping of the current sheet [Arridge et al., 2008a] also acts to push this boundary into the northern hemisphere for this particular set of observations which occurred at the end of southern summer and during equinox. This is clearly observed on the dayside latitudinal dependence (Figure 4b), where the regions of plasma depleted flux are observed at higher latitudes in the north than the southern dayside magnetosphere. A depletion in electron measurements at high latitudes is an indicator of where the magnetic field is open (where only one end of the magnetic field is tethered to the ionosphere). This is due to plasma being lost down the open field line if both footpoints of the

magnetospheric field are not at the ionosphere which will act to trap the plasma. Therefore, the region of depleted flux can be used to estimate where the magnetospheric field is open.

The observations were traced to the planet's surface, to estimate the invariant latitude (and colatitude) of where the depleted plasma is observed in the polar region. The open closed field line boundary (OCB) was estimated from individual high-latitude orbits using ELS measurements. The average invariant colatitude of the OCB was found to be located at colatitudes of 12.7±0.6º and 14.5+0.6º in the north and south, respectively. Our investigation includes the OCB identification for more orbits (86 crossings) than the Jinks et al., (2014) study (which analyzed 48 crossings). Our inclusion of more orbits indicates that Jinks et al., (2014) overestimated the location of the OCB with reported values of 13.3º and 15.6º for the north and south, respectively.

The average open flux content of the Saturnian magnetosphere was estimated to be 25±5 and 32±5 GWb for the northern and southern polar cap, respectively. These values are similar to the open flux estimates (10-50 GWb) calculated using auroral oval observations [Badman et al., 2014] and estimates from global MHD models for Saturn [20-35 GWb, Jia et al., 2012].

Finally, we have investigated the possibility of the invariant colatitude position of the OCB being modulated by the planetary period oscillations (PPOs). The PPOs consist of two independently rotating magnetic perturbation systems (one in the north and one in the south) that rotate at different periods [e.g. Andrews et al., 2012; Provan et al., 2016, 2018]. PPOs have been found to perturb and modulate many magnetospheric structures and processes in Saturn's magnetosphere including the auroral oval, dipolarizations in the magnetotail, as well as the plasma sheet [e.g. Nichols et al., 2008, 2016; Bader et al., 2019a; Bradley et al., 2018; Ramer et al., 2017; Thomsen et al., 2017]. Jinks et al., (2014) did not find a significant modulation of the OCB by PPO systems. We have found that by binning the data appropriately in local time longitudes to account for an average variation in the shape in local time of the OCB, the OCB in the north is weakly modulated by PPOs.

5 Conclusions

The whole electron measurement dataset from the spectrometer (ELS) onboard the Cassini spacecraft has been reduced to produce a signal-to-noise ratio. This has made it more straightforward to analyse the dataset as a whole in regards to when and where in the Saturnian magnetosphere plasma was observed with a high and low electron content. From our analysis we have found:

1) The most planetward reconnection x-line is located at 20 – 25 R_S downtail from the planet on the midnight to dawn side of the equatorial magnetosphere.

2) There is a local time (dawn-dusk) asymmetry. This may possibly indicate the presence of plasma depleted flux tubes returning to the dayside after reconnection.

3) A large volume of the high-latitude magnetosphere is in a state of constant plasma depletion and located on open field lines.

4) The average open flux content for the northern and southern polar caps are 25±5 and 32±5 GWb.

5) The average location of the open-closed field boundary is found at invariant colatitudes of 12.7±0.6º and 14.5±0.6º colatitude.

6) We have found that the northern open-closed field line boundary is weakly modulated by the northern PPO system.

The dataset is also ripe to be used in a variety of studies such as exploring the quasi-periodic 1hr pulsations (also known as QP60) that have also been observed at Saturn [e.g. Roussos et al., 2016]. Future work will include examining the cushion dawn region in more detail to confirm or deny the presence of this structure at Saturn. The open flux content also needs to be investigated in detail using both auroral observations and in situ observations together for individual Cassini orbits.

Figure 1. CAPS Electron Spectrometer (ELS) measurements during a high-latitude orbit passing through the magnetosphere, cusp and polar cap: a) electron differential energy flux ('DEF') summed over all 8 anodes, with the spacecraft ('s/c') potential and photoelectrons labeled; b) reduced electron spectrometer data showing the final signal-to-noise ratio ('SNR') described in the text (SNR=1 is shown by the dotted line). The cusp interval is analysed in detail by Jasinski et al., (2014).

Figure 2. ELS data in the equatorial (X_{KSMAG}-Y_{KSMAG}) plane, with the Sun to the right. The data shown is for locations within 5º in latitude and 2.5 R_S of the equator. The color scheme highlights when ELS measured electrons above background levels (white) and where it did not (red – for more details about the color scheme please Section 2.5). Grey shows where no data was taken. The orbit of Titan is shown at 20 R_S, and a model magnetopause is shown [Kanani et al., (2010)], which results in a standoff distance equal to ~27 R_S.

Figure 3. ELS data shown within 2.5 R_S of the warped current sheet model of Arridge et al., (2008). Left (a): equatorial plane in the same format as Figure 2. Crosses are of reconnection signatures reported by Smith et al., (2016). Right (b): The same dataset as a) but shown in local time (LT) and radial distance (R), highlighting a dawn-dusk asymmetry in the ELS observations.

Figure 4. ELS measurements in the high latitude magnetosphere during the highly-inclined orbits of 2006-2009. Left a): ELS data in the X_{KSMAG}-Z_{KSMAG} plane with the Sun to the right. Right b): Observations from the dayside magnetosphere (shown as radial distance and latitude).

Figure 5. ELS observations mapped to the (a) northern and (b) southern ionospheres. The three circles from the most poleward to the most equatorward are the statistical auroral oval locations for the poleward edge, center and equatorward edge, respectively, from (Bader et al., 2019a). Lines of local time longitude (dotted lines) are separated by 30º (2 hours LT), and dotted circles show colatitudes of 10º and 20º. Local times are labeled with 00 at midnight.

Figure 6. Open-closed field line boundary crossing by Cassini compared to the auroral oval position. Panel a): mapped location of Cassini (red, for the northern interval shown in the spectrogram) in the northern polar cap and the location of the OCB (blue star), model OCB oval (blue) observed on 04 Jan 2009 at 04:20 UT, with the statistical location of the auroral oval from Bader et al., (2019a). Local time longitudes gridlines separated by 2 hours LT (or 30º) and colatitudes of 10º are shown. Panel b) UVIS auroral observations of the northern aurora on 04 Jan 2009 at 09:45 UT, with the mapped location of Cassini (yellow diamond) during the UVIS observations (and the OCB crossing – blue star) as well as Cassini's trajectory. The northern (red) and southern (blue) longitudinal PPO positions are shown. Panel c-d) Cassini's radial distance from Saturn and magnetic latitude are shown, respectively. Panel e-f) signal-to-noise ratio (SNR) and spectrogram measured by ELS during the interval shown in panel a). The spacecraft potential is shown as the black line in panel f). The dashed vertical lines show the selection of the open-closed field line boundary.

Figure 7. Open-closed field line boundary (OCB) location and PPO modulation. Panel a-b) the invariant colatitude location shown for different Cassini orbits (Revs), and c-d) for different local times, with the average auroral oval from Bader et al., (2019a). Panel e-h) Displacement of the OCB invariant colatitude (Λ) depending on PPO magnetic longitude $\Psi_{N/S}$ ($\Psi_{S/N}$) for the northern OCB (southern). The best fit model and corresponding goodness-of-fit (χ^2) is also shown.

Acknowledgments, Samples, and Data

JMJ was supported by an appointment to the NASA Postdoctoral Program at the Jet Propulsion Laboratory administered by Universities Space Research Association (USRA) through a contract with the National Aeronautics and Space Administration (NASA). AB was funded by a Lancaster University FST studentship. NM acknowledges support from the Jet Propulsion Laboratory, California Institute of Technology, under a contract with NASA. AJC acknowledges STFC support via the solar system consolidated grant to UCL-MSSL. PPO data can be found at https://lra.le.ac.uk/handle/2381/42436. All the data used in this study can be found at NASA's Planetary Data System (https://pds.jpl.nasa.gov).

References

Achilleos, N., André, N., Blanco- Cano, X., Brandt, P. C., Delamere, P. A., & Winglee, R. (2015). 1. Transport of mass, momentum and energy in planetary magnetodisc regions. *Space Science Reviews*, **187**(1–4), 229–299. https://doi.org/10.1007/s11214- 014- 0086- y

Andrews, D. J., Cowley, S. W. H., Dougherty, M. K., & Provan, G. (2010). Magnetic field oscillations near the planetary period in Saturn's equatorial magnetosphere: Variation of amplitude and phase with radial distance and local time. *Journal of Geophysical Research*, **115**, A04212. https://doi.org/10.1029/2009JA014729

Andrews, D. J., Cowley, S. W. H., Dougherty, M. K., Lamy, L., Provan, G., & Southwood, D. J. (2012).Planetary period oscillations in Saturn's magnetosphere: Evolution of magnetic oscillation properties from southern summer to post- equinox. *Journal of Geophysical Research*, **117**, A04224. https://doi.org/10.1029/2011JA017444

Andriopoulou, M., Roussos, E., Krupp, N., Paranicas, C., Thomsen, M., Krimigis, S., Dougherty, M. K., and Glassmeier, K.- H. (2012), A noon- to- midnight electric field and nightside dynamics in Saturn's inner magnetosphere, using microsignature observations, *Icarus*, 220, 503– 513, doi:10.1016/j.icarus.2012.05.010.

Andriopoulou, M., Roussos, E., Krupp, N., Paranicas, C., Thomsen, M., Krimigis, S., Dougherty, M. K., and Glassmeier, K.- H. (2014), Spatial and temporal dependence of the convective electric field in Saturn's inner magnetosphere, *Icarus*, 229, 57– 70, doi:10.1016/j.icarus.2013.10.028.

Arnold, H., Swisdak, M., & Drake, J. F. (2018). Characterizing ion flows across a magnetotail dipolarization jet. *Journal of Geophysical Research: Space Physics*, 123, 6326– 6334. https://doi.org/10.1029/2018JA025604

Arridge, C. S., Khurana, K. K., Russell, C. T., Southwood, D. J., Achilleos, N., Dougherty, M. K., Coates, A. J., and Leinweber, H. K. (2008a), Warping of Saturn's magnetospheric and magnetotail current sheets, *J. Geophys. Res.*, **113**, A08217, doi:10.1029/2007JA012963.

Arridge, C. S., Russell, C. T., Khurana, K. K., Achilleos, N., Cowley, S. W. H., Dougherty, M. K.,Southwood, D. J., and Bunce, E. J. (2008b), Saturn's

magnetodisc current sheet, *J. Geophys. Res.*,**113**, A04214, doi:10.1029/2007JA012540.

Arridge, C. S., et al. (2009), Plasma electrons in Saturn's magnetotail: Structure, distribution and energisation, *Planet. Space Sci.*, **57**(14–15), 2032– 2047, doi:10.1016/j.pss.2009.09.007.

Arridge, C.S., André, N., McAndrews, H.J. et al. Space Sci Rev (2011a) 164: 1. https://doi.org/10.1007/s11214-011-9850-4

Arridge, C. S., et al. (2011b), Periodic motion of Saturn's nightside plasma sheet, *J. Geophys. Res.*,**116**, A11205, doi:10.1029/2011JA016827.

Arridge, C. S., Kane, M., Sergis, N., Khurana, K. K., and Jackman, C. J. (2015), Sources of local time asymmetries in magnetodiscs, *Space Sci. Rev.*, **187**, 301– 333.

Arridge, C. S., Jasinski, J. M., Achilleos, N., Bogdanova, Y. V., Bunce, E. J., Cowley, S. W. H., Fazakerley, A. N., Khurana, K. K., Lamy, L., Leisner, J. S., et al. (2016a), Cassini observations of Saturn's southern polar cusp, *J. Geophys. Res. Space Physics*, 121, 3006– 3030, doi:10.1002/2015JA021957.

Arridge, C. S., et al. (2016b), Cassini in situ observations of long- duration magnetic reconnection in Saturn's magnetotail, *Nat. Phys.*, **12**, 268– 271.

André, N., Persoon, A. M., Goldstein, J., Burch, J. L., Louarn, P., Lewis, G. R., et al. (2007). Magnetic signatures of plasma- depleted flux tubes in the Saturnian inner magnetosphere. *Geophysical Research Letters*, **34**, L14108. https://doi.org/10.1029/2007GL030374

Azari, A. R., Liemohn, M. W., Jia, X., Thomsen, M. F., Mitchell, D. G., Sergis, N., et al. (2018). Interchange injections at Saturn: Statistical survey of energetic H^+ sudden flux intensifications. *Journal of Geophysical Research: Space Physics*, 123, 4692– 4711. https://doi.org/10.1029/2018JA025391

Azari, A. R., Jia, X., Liemohn, M. W., Hospodarsky, G. B., Provan, G., Ye, S.- Y., et al. (2019). Are Saturn's interchange injections organized by rotational longitude? *Journal of Geophysical Research: Space Physics*,124, 1806– 1822

Bader, A., Badman, S. V., Kinrade, J., Cowley, S. W. H., Provan, G., & Pryor, W. R. (2018). Statistical planetary period oscillation signatures in Saturn's UV auroral intensity. *Journal of Geophysical Research: Space Physics*, 123, 8459– 8472. https://doi.org/10.1029/2018JA025855

Bader, A., Badman, S. V., Kinrade, J., Cowley, S. W. H., Provan, G., & Pryor, W. (2019a). Modulations of Saturn's UV auroral oval location by planetary period

oscillations. *Journal of Geophysical Research: Space Physics*, 124, 952–970. https://doi.org/10.1029/2018JA026117

Bader, A., Badman, S. V., Yao, Z. H., Kinrade, J., & Pryor, W. R. (2019b). Observations of continuous quasiperiodic auroral pulsations on Saturn in high time- resolution UV auroral imagery. *Journal of Geophysical Research: Space Physics*, 124, 2451–2465. https://doi.org/10.1029/2018JA026320

Badman, S. V., Bunce, E. J., Clarke, J. T., Cowley, S. W. H., Gérard, J.- C., Grodent, D., and Milan, S. E. (2005), Open flux estimates in Saturn's magnetosphere during the January 2004 Cassini- HST campaign, and implications for reconnection rates, *J. Geophys. Res.*, 110, A11216, doi:10.1029/2005JA011240.

Badman, S. V., Andrews, D. J., Cowley, S. W. H., Lamy, L., Provan, G., Tao, C., et al. (2012).Rotational modulation and local time dependence of Saturn's infrared H_3^+ auroral intensity. *Journal of Geophysical Research*, **117**, A09228. https://doi.org/10.1029/2011JA017990

Badman, S. V., Masters, A., Hasegawa, H., Fujimoto, M., Radioti, A., Grodent, D., Sergis, N.,Dougherty, M. K., and Coates, A. J. (2013), Bursty magnetic reconnection at Saturn's magnetopause, *Geophys. Res. Lett.*, **40**, 1027– 1031, doi:10.1002/grl.50199.

Badman, S. V., C. M. Jackman, J. D. Nichols, J. T. Clarke, and J.-C. G´erard (2014), Open flux in Saturn's magnetosphere, Icarus, 231, 137–145, doi:10.1016/j.icarus.2013.12.004.

Balogh, A., Dougherty, M. K., Forsyth, R. J., Southwood, D. J., Smith, E. J., Tsurutani, B. T.,
et al. (1992). Magnetic field observations during the Ulysses flyby of Jupiter. *Science*, **257**(5076), 1515–1518. https://doi.org/10.1126/science.257.5076.1515

Bradley, T. J., Cowley, S. W. H., Bunce, E. J., Smith, A. W., Jackman, C. M., & Provan, G. (2018). Planetary period modulation of reconnection bursts in Saturn's magnetotail. *Journal of Geophysical Research: Space Physics*, 123, 9476–9507. https://doi.org/10.1029/2018JA025932

Bunce, E. J., Cowley, S. W. H., Wright, D. M., Coates, A. J., Dougherty, M. K., Krupp, N., Kurth, W. S., and Rymer, A. M. (2005), In situ observations of a solar wind compression- induced hot plasma injection in Saturn's tail, *Geophys. Res. Lett.*, **32**, L20S04, doi:10.1029/2005GL022888.

Bunce, E. J., S. W. H. Cowley, I. I. Alexeev, C. S. Arridge, M. K. Dougherty, J. D. Nichols, and C. T. Russell (2007), Cassini observations of the variation of Saturn's ring current parameters with system size, J. of Geophys. Res., 112, A10202, doi:10.1029/2007JA012275.

Bunce, E. J., C. S. Arridge, J. T. Clarke, A. J. Coates, S. W. H. Cowley, M. K. Dougherty, J.-C. G´erard, D. Grodent, K. C. Hansen, J. D. Nichols, D. J. Southwood, and D. L. Talboys (2008b), Origin of Saturn's aurora: Simultaneous observations by Cassini and the Hubble Space Telescope, J. Geophys. Res., 113(12), A09209, doi:10.1029/2008JA013257.

Burch, J. L., Goldstein, J., Hill, T. W., Young, D. T., Crary, F. J., Coates, A. J., et al. (2005). Properties of local plasma injections in Saturn's magnetosphere. *Geophysical Research Letters*, **32**, L14S02. https://doi.org/10.1029/2005GL022611

Burton, M. E., M. K. Dougherty, and C. T. Russell (2010), Saturn's internal plane- tary magnetic field, Geophys. Res. Lett., 37, L24105, doi:10.1029/2010GL045148.

Carbary, J. F., Achilleos, N., and Arridge, C. S. (2012), Statistical ring current of Saturn, *J. Geophys. Res.*, **117**, A06223, doi:10.1029/2011JA017472.

Carbary, J. F., & Mitchell, D. G. (2013). Periodicities in Saturn's magnetosphere. *Reviews of Geophysics*, **51**, 1–30. https://doi.org/10.1002/rog.20006

Carbary, J. F. (2017), Update on Saturn's energetic electron periodicities, *J. Geophys. Res. Space Physics*,122, 156– 165, doi:10.1002/2016JA023405.

Carbary J. F., Magnetodisk Coordinates for Saturn, *Journal of Geophysical Research: Space Physics*, **124**, 1, (451-458), (2019).

Clarke, K. E., Andrews, D. J., Arridge, C. S., Coates, A. J., & Cowley, S. W. H. (2010). Magnetopause oscillations near the planetary period at Saturn: Occurrence, phase, and amplitude. *Journal of Geophysical Research*, **115**, A08209. https://doi.org/10.1029/2009JA014745

Connerney, J. E. P., M. H. Acuna, and N. F. Ness (1981), Modeling the Jovian current sheet and inner magnetosphere, J. Geophys. Res., 86, 8370–8384, doi: 10.1029/JA086iA10p08370.

Connerney, J. E. P., Acuña, M. H., and Ness, N. F. (1983), Currents in Saturn's magnetosphere, *J. Geophys. Res.*, **88**(A11), 8779– 8789.

Cowley, S. W. H., and E. J. Bunce (2003), Corotation-driven magnetosphere-ionosphere coupling currents in saturns magnetosphere and their rela- tion to the auroras, Annales Geophysicae, 21(8), 1691–1707, doi:10.5194/ angeo-21-1691-2003.

Cowley, S. W. H., S. V. Badman, E. J. Bunce, J. T. Clarke, J.-C. G´erard, D. Grodent, C. M. Jackman, S. E. Milan, and T. K. Yeoman (2005), Reconnection in a rotation dominated magnetosphere and its relation to Saturn's auroral dynamics, J.

Geophys. Res., 110, A02201, doi:10.1029/2004JA010796.

Dewey, R. M., Slavin, J. A., Raines, J. M., Baker, D. N., & Lawrence, D. J. (2017). Energetic electron acceleration and injection during dipolarization events in Mercury's magnetotail. *Journal of Geophysical Research: Space Physics*, 122, 12,170– 12,188. https://doi.org/10.1002/2017JA024617

Dougherty, M. K., et al. (2004), The Cassini magnetic field investigation, *Space Sci. Rev.*, **114**, 331– 383, doi:10.1007/s11214-004-1432-2

Dougherty MK, et al. (2018) Saturn's magnetic field revealed by the Cassini Grand Finale. Science 362:eaat5434.

Dungey, J. W. (1961), Interplanetary Magnetic Field and the Auroral Zones, Phys. Rev. Lett., 6, 47–48, doi:10.1103/PhysRevLett.6.47.

Felici, M., Arridge, C. S., Wilson, R. J., Coates, A. J., Thomsen, M., & Reisenfeld, D. (2018).Survey of thermal plasma composition in Saturn's magnetosphere using time-of-flight data from Cassini/CAPS. *Journal of Geophysical Research: Space Physics*, 123, 6494– 6513. https://doi.org/10.1029/2017JA025085

Fu, Z. F., and Lee, L. C. (1985), Simulation of multiple X- line reconnection at the dayside magnetopause, *Geophys. Res. Lett.*, **12**(5), 291– 294, doi:10.1029/GL012i005p00291.

Fuselier, S. A., Frahm, R., Lewis, W. S., Masters, A., Mukherjee, J., Petrinec, S. M., and Sillanpaa, I. J. (2014), The location of magnetic reconnection at Saturn's magnetopause: A comparison with Earth, *J. Geophys. Res. Space Physics*, **119**, 2563– 2578, doi:10.1002/2013JA019684.

Gershman, D. J., DiBraccio, G. A., Connerney, J. E. P., Bagenal, F., Kurth, W. S., Hospodarsky, G. B., et al. (2018). Juno constraints on the formation of Jupiter's magnetospheric cushion region. *Geophysical Research Letters*, 45, 9427– 9434. https://doi.org/10.1029/2018GL079118

Giampieri, G., and Dougherty, M. K. (2004), Modelling of the ring current in Saturn's magnetosphere, *Ann. Geophys.*, **22**, 653– 659.

Guo, R. L., Yao, Z. H., Wei, Y., Ray, L. C., Rae, I. J., Arridge, C. S., Coates, A. J., Delamere, P. A., Sergis, N., Kollmann, P., Grodent, D., Dunn, W. R., Waite, J. H., Burch, J. L., Pu, Z. Y., Palmaerts, B.,Dougherty, M. K. (2018a). Rotationally driven magnetic reconnection in Saturn's dayside. *Nature Astronomy*, **2**(8), 640– 645. https://doi.org/10.1038/s41550-018-0461-9

Guo, R. L., et al., Reconnection Acceleration in Saturn's Dayside Magnetodisk: A Multicase Study with Cassini (2018b), Ap. J. Letters, Vol. 868, Number 2,

doi:10.3847/2041-8213

Hill, T. W., Rymer, A. M., Burch, J. L., Crary, F. J., Young, D. T., Thomsen, M. F., et al. (2005). Evidence for rotationally driven plasma transport in Saturn's magnetosphere. *Geophysical Research Letters*,**32**, L14S10. https://doi.org/10.1029/2005GL022620

Hill, T. W., et al. (2008), Plasmoids in Saturn's magnetotail, *J. Geophys. Res.*, **113**, A01214, doi:10.1029/2007JA012626.

Hones, E. W. (1976), The magnetotail—Its generation and dissipation, *Phys. Sol. Planet. Environ.*, **2**,558– 571.

Hunt, G. J., Cowley, S. W. H., Provan, G., Bunce, E. J., Alexeev, I. I., Belenkaya, E. S., Kalegaev, V. V.,Dougherty, M. K., Coates, A. J. (2014). Field- aligned currents in Saturn's southern nightside magnetosphere: Subcorotation and planetary period oscillation components. *Journal of Geophysical Research: Space Physics*, **119**, 9847– 9899. https://doi.org/10.1002/2014JA020506

Hunt, G. J., Cowley, S. W. H., Provan, G., Bunce, E. J., Alexeev, I. I., Belenkaya, E. S., Kalegaev, V. V.,Dougherty, M. K., Coates, A. J. (2015). Field- aligned currents in Saturn's northern nightside magnetosphere: Evidence for interhemispheric current flow associated with planetary period oscillations. *Journal of Geophysical Research: Space Physics*, **120**, 7552– 7584. https://doi.org/10.1002/2015JA021454

Hunt, G. J., Cowley, S. W. H., Provan, G., Bunce, E. J., Alexeev, I. I., Belenkaya, E. S., Kalegaev, V. V.,Dougherty, M. K., Coates, A. J. (2016). Field- aligned currents in Saturn's magnetosphere: Local time dependence of southern summer currents in the dawn sector between midnight and noon. *Journal of Geophysical Research: Space Physics*, **121**, 7785– 7804. https://doi.org/10.1002/2016JA022712

Ieda, A., Machida, S., Mukai, T., Saito, Y., Yamamoto, T., Nishida, A., Terasawa, T., and Kokubun, S.(1998), Statistical analysis of the plasmoid evolution with geotail observations, *J. Geophys. Res.*, **103**(A3), 4453– 4465, doi:10.1029/97JA03240.

Jackman, C. M., et al. (2014), Saturn's dynamic magnetotail: A comprehensive magnetic field and plasma survey of plasmoids and traveling compression regions and their role in global magnetospheric dynamics, *J. Geophys. Res. Space Physics*, **119**, 5465– 5494, doi:10.1002/2013JA019388.

Jackman, C. M., Provan, G., & Cowley, S. W. H. (2016). Reconnection events in Saturn's magnetotail: Dependence of plasmoid occurrence on planetary period oscillation phase. *Journal of Geophysical Research: Space Physics*, **121**, 2922– 2934. https://doi.org/10.1002/2015JA021985

Jasinski, J. M., et al. (2014), Cusp observation at Saturn's high- latitude magnetosphere by the Cassini spacecraft, *Geophys. Res. Lett.*, **41**, 1382– 1388, doi:10.1002/2014GL059319.

Jasinski, J. M., Christopher S. Arridge, Andrew J. Coates, Geraint H. Jones, Nick Sergis, Michelle F. Thomsen, Daniel B. Reisenfeld, Norbert Krupp and J. Hunter Waite, Cassini plasma observations of Saturn's magnetospheric cusp, *Journal of Geophysical Research: Space Physics*, **121**, 12, (12,047-12,067), (2016).

Jasinski, J. M., James A. Slavin, Christopher S. Arridge, Gangkai Poh, Xianzhe Jia, Nick Sergis, Andrew J. Coates, Geraint H. Jones and J. Hunter Waite, Flux transfer event observation at Saturn's dayside magnetopause by the Cassini spacecraft, *Geophysical Research Letters*, **43**, 13, (6713-6723), (2016).

Jasinski, J. M., Christopher S. Arridge, Andrew J. Coates, Geraint H. Jones, Nick Sergis, Michelle F. Thomsen and Norbert Krupp, Diamagnetic depression observations at Saturn's magnetospheric cusp by the Cassini spacecraft, *Journal of Geophysical Research: Space Physics*, **122**, 6, (6283-6303), (2017a).

Jasinski, J. M., Slavin, J. A., Raines, J. M., & DiBraccio, G. A. (2017b). Mercury's solar wind interaction as characterized by magnetospheric plasma mantle observations with MESSENGER. *Journal of Geophysical Research: Space Physics*, 122, 12,153– 12,169. https://doi.org/10.1002/2017JA024594

Jia, X., Hansen, K. C., Gombosi, T. I., Kivelson, M. G., Tóth, G., DeZeeuw, D. L., and Ridley, A. J. (2012), Magnetospheric configuration and dynamics of Saturn's magnetosphere: A global MHD simulation, *J. Geophys. Res.*, **117**, A05225, doi:10.1029/2012JA017575.

Jia, X., and Kivelson, M. G. (2016), Dawn- dusk asymmetries in rotating magnetospheres: Lessons from modeling Saturn, *J. Geophys. Res. Space Physics*, 121, 1413– 1424, doi:10.1002/2015JA021950.

Jinks, S. L., et al. (2014), Cassini multi- instrument assessment of Saturn's polar cap boundary, *J. Geophys. Res. Space Physics*, **119**, 8161– 8177, doi:10.1002/2014JA020367.

JohnstoneA.D., C. Alsop, S. Burge, P.J. Carter, A.J. Coates, A.J. Coker, A.N. Fazakerle y, M. Grande, R.A. Gowen, C. Gurgiolo, B.K. Hancock, B. Narheim, A.Preece, P.H. Sheather, J.D. Winningham, R.D. Woodliffe, Peace: A plasma electron and current experiment Space Sci. Rev., 79 (1997), pp. 351-398

Jones, G. H., E. Roussos, N. Krupp, C. Paranicas, J. Woch, A. Lagg, D. G. Mitchell, S. M. Krimigis, and M. K. Dougherty (2006), Enceladus' Varying Imprint on the Magnetosphere of Saturn, Science, 311, 1412–1415,

doi:10.1126/science.1121011.

Kellett, S., Bunce, E. J., Coates, A. J., and Cowley, S. W. H. (2009), Thickness of Saturn's ring current determined from north- south Cassini passes through the current layer, *J. Geophys. Res.*, **114**, A04209, doi:10.1029/2008JA013942.

Kellett, S., Arridge, C. S., Bunce, E. J., Coates, A. J., Cowley, S. W. H., Dougherty, M. K., Persoon, A. M.,Sergis, N., and Wilson, R. J. (2011), Saturn's ring current: Local time dependence and temporal variability, *J. Geophys. Res.*, **116**, A05220, doi:10.1029/2010JA016216.

Kennelly, T. J., Leisner, J. S., Hospodarsky, G. B., & Gurnett, D. A. (2013). Ordering of injection events within Saturnian SLS longitude and local time. *Journal of Geophysical Research: Space Physics*, **118**, 832–838. https://doi.org/10.1002/jgra.50152

Kinrade, J., et al. (2017), An isolated, bright cusp aurora at Saturn, *J. Geophys. Res. Space Physics*, 122,6121– 6138, doi:10.1002/2016JA023792.

Kivelson, M. G., Khurana, K. K., Russell, C. T., Walker, R. J., Coleman, P. J., Coroniti, F. V., et al. (1997). Galileo at Jupiter: Changing states of the magnetosphere and first looks at Io and Ganymede. *Advances in Space Research*, **20**(2), 193–204. https://doi.org/10.1016/S0273- 1177(97)00533- 4

Kivelson, M. G., & Southwood, D. J. (2005). Dynamical consequences of two modes of centrifugal instability in Jupiter's outer magnetosphere. *Journal of Geophysical Research*, **110**, A12209. https://doi.org/10.1029/2005JA011176

Krupp, N., E. Roussos, H. Kriegel, P. Kollmann, M. G. Kivelson, A. Kotova, C. Paranicas,D. G. Mitchell, S. M. Krimigis, and K. K. Khurana (2013), Energetic particle measurements in the vicinity of Dione during the three Cassini encounters 2005–2011, *Icarus*, 2013, 617− 628.

Lai, H. R., Russell, C. T., Jia, Y. D., Wei, H. Y., & Dougherty, M. K. (2016). Transport of magnetic flux and mass in Saturn's inner magnetosphere. *Journal of Geophysical Research: Space Physics*, **121**,790– 803. https://doi.org/10.1002/2015JA021980

Lewis, G. R., C. S. Arridge, D. R. Linder, L. K. Gilbert, D. O. Kataria, A. J. Coates, A. Persoon, G. A. Collinson, N. Andr´e, P. Schippers, J. Wahlund, M. Morooka, G. H. Jones, A. M. Rymer, D. T. Young, D. G. Mitchell, A. Lagg, and S. A. Livi (2010), The calibration of the Cassini-Huygens CAPS Electron Spectrometer, Planet. Space Sci., 58, 427–436, doi:10.1016/j.pss.2009.11.008.

Lewis,G.R., N. André, C.S. Arridge, A.J. Coates, L.K. Gilbert, D.R. Linder, A.M.Rymer Derivation of density and temperature from the Cassini-Huygens CAPS Electron

Spectrometer, Planet. Space Sci., 56 (7) (2008), pp. 901-912, 10.1016/j.pss.2007.12.017

Linder, D. R., A. J. Coates, R. D. Woodliffe, C. Alsop, A. D. Johnstone, M. Grande, A. Preece, B. Narheim, and D. T. Young (1998), The Cassini CAPS Electron Spectrometer, Washington DC American Geophysical Union Geophysical Monograph Series, 102, 257.

Masters, A., et al. (2012), The importance of plasma *β* conditions for magnetic reconnection at Saturn's magnetopause, *Geophys. Res. Lett.*, **39**, L08103, doi:10.1029/2012GL051372

Martin, C. J., & Arridge, C. S (2017). Cassini observations of aperiodic waves on Saturn's equatorial current sheet. *Journal of Geophysical Research: Space Physics*, **122**, 8063– 8077.

Nichols, J. D., Clarke, J. T., Cowley, S. W. H., Duval, J., Farmer, A. J., Gérard, J.-C., Grodent, D., andWannawichian, S. (2008), Oscillation of Saturn's southern auroral oval, *J. Geophys. Res.*, 113, A11205, doi:10.1029/2008JA013444.

Nichols, J. D., Badman, S. V., Bunce, E. J., Clarke, J. T., Cowley, S. W. H., Hunt, G. J., & Provan, G. (2016). Saturn's northern auroras as observed using the Hubble Space Telescope. *Icarus*, **263**, 17– 31. https://doi.org/10.1016/j.icarus.2015.09.008

Palmaerts, A. Radioti, E. Roussos, D. Grodent, J.- C. Gérard, N. Krupp and D. G. Mitchell, Pulsations of the polar cusp aurora at Saturn, *Journal of Geophysical Research: Space Physics*, **121**, 12, (11,952-11,963), (2016).

Paranicas, C., Mitchell, D. G., Roelof, E. C., Brandt, P. C., Williams, D. J., Krimigis, S. M., and Mauk, B. H. (2005), Periodic intensity variations in global ENA images of Saturn, *Geophys. Res. Lett.*, 32, L21101, doi:10.1029/2005GL023656.

Paranicas, C., Thomsen, M. F., Achilleos, N., Andriopoulou, M., Badman, S. V., Hospodarsky, G., et al. (2016). Effects of radial motion on interchange injections at Saturn. *Icarus*, **264**, 342– 351.

Paschmann, G., Fazakerley, A.N., Schwartz, S.J., 2000. Analysis Methods for MultiSpacecraft Data, ISSI/ESA, pp. 125–157 (Ch. Moments of Plasma Velocity Distributions)

Provan, G., Andrews, D. J., Cecconi, B., Cowley, S. W. H., Dougherty, M. K., Lamy, L., & Zarka, P. M. (2011). Magnetospheric period magnetic field oscillations at Saturn: Equatorial phase “jitter” produced by superposition of southern and northern period oscillations. *Journal of Geophysical Research*, **116**, A04225. https://doi.org/10.1029/2010JA016213

Provan, G., Tao, C., Cowley, S. W. H., Dougherty, M. K., & Coates, A. J. (2015). Planetary period oscillations in Saturn's magnetosphere: Examining the relationship between abrupt changes in behavior and solar wind- induced magnetospheric compressions and expansions. *Journal of Geophysical Research: Space Physics*, **120**, 9524– 9544. https://doi.org/10.1002/2015JA021642

Provan, G., Cowley, S. W. H., Lamy, L., Bunce, E. J., Hunt, G. J., Zarka, P., & Dougherty, M. K. (2016).Planetary period oscillations in Saturn's magnetosphere: Coalescence and reversal of northern and southern periods in late northern spring. *Journal of Geophysical Research: Space Physics*, **121**,9829– 9862. https://doi.org/10.1002/2016JA023056

Provan, G., Cowley, S. W. H., Bradley, T. J., Bunce, E. J., Hunt, G. J., & Dougherty, M. K. (2018).Planetary period oscillations in Saturn's magnetosphere: Cassini magnetic field observations over the northern summer solstice interval. *Journal of Geophysical Research: Space Physics*, **123**, 3859– 3899. https://doi.org/10.1029/2018JA025237

Radioti, A., Grodent, D., Gérard, J.- C., Milan, S. E., Bonfond, B., Gustin, J., and Pryor, W. (2011),Bifurcations of the main auroral ring at Saturn: ionospheric signatures of consecutive reconnection events at the magnetopause, *J. Geophys. Res.*, 116, A11209, doi:10.1029/2011JA016661.

Radioti, A., Grodent, D., Gérard, J.- C., Bonfond, B., Gustin, J., Pryor, W., Jasinski, J. M., and Arridge, C. S. (2013), Auroral signatures of multiple magnetopause reconnection at Saturn, *Geophys. Res. Lett.*,**40**, 4498– 4502, doi:10.1002/grl.50889.

Ramer, K. M., Kivelson, M. G., Sergis, N., Khurana, K. K., & Jia, X. (2017). Spinning, breathing, and flapping: Periodicities in Saturn's middle magnetosphere. *Journal of Geophysical Research: Space Physics*, **122**, 393– 416. https://doi.org/10.1002/2016JA023126

Roussos, E., Kollmann, P., Krupp, N., Paranicas, C., Krimigis, S. M., Mitchell, D. G., Holmbergi, K. G. (2012). Energetic electron observations of Rhea's magnetospheric interaction. *Icarus*, 221, 116– 134.

Roussos, E., Krupp, N., Mitchell, D., Paranicas, C., Krimigis, S., Andriopoulou, M., & Dougherty, M. (2016). Quasi- periodic injections of relativistic electrons in Saturn's outer magnetosphere. *Icarus*,**263**, 101– 116. https://doi.org/10.1016/j.icarus.2015.04.017

Rymer, A. M., Mauk, B. H., Hill, T. W., André, N., Mitchell, D. G., Paranicas, C., et al. (2009). Cassini evidence for rapid interchange transport at Saturn. *Planetary and Space Science*, **57**(14–15), 1779– 1784. https://doi.org/10.1016/j.pss.2009.04.010

Sergis, N., Krimigis, S. M., Mitchell, D. G., Hamilton, D. C., Krupp, N., Mauk, B. H., Roelof, E. C., andDougherty, M. K. (2009), Energetic particle pressure in Saturn's magnetosphere measured with the Magnetospheric Imaging Instrument on Cassini, *J. Geophys. Res.*, **114**, A02214, doi:10.1029/2008JA013774.

Sergis, N., Arridge, C. S., Krimigis, S. M., Mitchell, D. G., Rymer, A. M., Hamilton, D. C., Krupp, N.,Dougherty, M. K., and Coates, A. J. (2011), Dynamics and seasonal variations in Saturn's magnetospheric plasma sheet, as measured by Cassini, *J. Geophys. Res.*, **116**, A04203, doi:10.1029/2010JA016180.

Sergis, N., Jackman, C. M., Thomsen, M. F., Krimigis, S. M., Mitchell, D. G., Hamilton, D. C., Dougherty, M. K., Krupp, N., and Wilson, R. J. (2017), Radial and local time structure of the Saturnian ring current, revealed by Cassini, *J. Geophys. Res. Space Physics*, 122, 1803– 1815, doi:10.1002/2016JA023742.

Slavin, J. A., Fairfield, D. H., Lepping, R. P., Hesse, M., Ieda, A., Tanskanen, E., Østgaard, N., Sutcliffe, P. R. (2002), Simultaneous observations of earthward flow bursts and plasmoid ejection during magnetospheric substorms, *Journal of Geophysical Research*, **107**(A7), 1106.

Slavin, J. A., et al. (2012a), MESSENGER observations of a flux- transfer- event shower at Mercury, *J. Geophys. Res.*, **117**, A00M06, doi:10.1029/2012JA017926

Slavin, J. A., Anderson, B. J., Baker, D. N., Benna, M., Boardsen, S. A., Gold, R. E., … Zurbuchen, T. H.(2012b). MESSENGER and Mariner 10 flyby observations of magnetotail structure and dynamics at Mercury. *Journal of Geophysical Research*, **117**, A01215. https://doi.org/10.1029/2011JA016900

Slavin, J. A., et al. (2014), MESSENGER observations of Mercury's dayside magnetosphere under extreme solar wind conditions, *J. Geophys. Res. Space Physics*, **119**, 8087– 8116, doi:10.1002/2014JA020319.

Smith, E. J., Davis, L., Jones, D. E., Coleman, P. J., Colburn, D. S., Dyal, P., et al. (1974). The planetary magnetic field and magnetosphere of Jupiter: Pioneer 10. *Journal of Geophysical Research*, **79**(25),3501– 3513. https://doi.org/10.1029/JA079i025p03501

Smith, E. J., Davis, L., & Jones, D. E. (1976). Jupiter's magnetic field and magnetosphere. In *Jupiter*, (pp. 788– 829). Tucson: Univ. of Ariz. Press.

Smith, A. W., C. M. Jackman, and M. F. Thomsen (2016), Magnetic reconnection in Saturn’s magnetotail: A comprehensive magnetic field survey, J. Geophys. Res. Space Physics, 121, 2984–3005, doi:10.1002/2015JA022005.

Smith, A. W., Jackman, C. M., Thomsen, M. F., Lamy, L., & Sergis, N. (2018a). Multi-instrument investigation of the location of Saturn's magnetotail x- line. *Journal of Geophysical Research: Space Physics*, 123, 5494–5505. https://doi.org/10.1029/2018JA025532

Smith, A. W., Jackman, C. M., Thomsen, M. F., Sergis, N., Mitchell, D. G., & Roussos, E. (2018b).Dipolarization fronts with associated energized electrons in Saturn's magnetotail. *Journal of Geophysical Research: Space Physics*, 123, 2714–2735. https://doi.org/10.1002/2017JA024904

Sorba, A. M., Achilleos, N. A., Guio, P., Arridge, C. S., Sergis, N., & Dougherty, M. K. (2018). The periodic flapping and breathing of Saturn's magnetodisk during equinox. *Journal of Geophysical Research: Space Physics*, 123, 8292–8316. https://doi.org/10.1029/2018JA025764

Southwood, D. J., and Kivelson, M. G. (1987), Magnetospheric interchange instability, *J. Geophys. Res.*,92(A1), 109– 116, doi:10.1029/JA092iA01p00109.

Swisdak, M., Rogers, B. N., Drake, J. F., and Shay, M. A. (2003), Diamagnetic suppression of component magnetic reconnection at the magnetopause, *J. Geophys. Res.*, **108**, 1218, doi:10.1029/2002JA009726.

Swisdak, M., Opher, M., Drake, J. F., and Alouani Bibi, F. (2010), The vector direction of the interstellar magnetic field outside the heliosphere, *Astrophys. J.*, **710**, 1769–1775, doi:10.1088/0004-637X/710/2/1769.

Thomsen, M. F., Reisenfeld, D. B., Delapp, D. M., Tokar, R. L., Young, D. T., Crary, F. J., et al. (2010).Survey of ion plasma parameters in Saturn's magnetosphere. *Journal of Geophysical Research*, **115**, A10220. https://doi.org/10.1029/2010JA015267

Thomsen, M. F., Roussos, E., Andriopoulou, M., Kollmann, P., Arridge, C. S., Paranicas, C. P., Gurnett, D. A., Powell, R. L., Tokar, R. L., and Young, D. T. (2012), Saturn's inner magnetospheric convection pattern: Further evidence, *J. Geophys. Res.*, 117, A09208, doi:10.1029/2011JA017482

Thomsen, M. F., Wilson, R. J., Tokar, R. L., Reisenfeld, D. B., and Jackman, C. M. (2013),Cassini/CAPS observations of duskside tail dynamics at Saturn, *J. Geophys. Res. Space Physics*, **118**,5767– 5781, doi:10.1002/jgra.50552.

Thomsen, M. F., Reisenfeld, D. B., Wilson, R. J., Andriopoulou, M., Crary, F. J., Hospodarsky, G. B., et al. (2014). Ion composition in interchange injection events in Saturn's magnetosphere. *Journal of Geophysical Research: Space Physics*, **119**, 9761– 9772.

Thomsen, M. F., Jackman, C. M., Cowley, S. W. H., Jia, X., Kivelson, M. G., & Provan, G. (2017).Evidence for periodic variations in the thickness of Saturn's nightside plasma sheet. *Journal of Geophysical Research: Space Physics*, **122**, 280– 292. https://doi.org/10.1002/2016JA023368

Tokar, R. L., R. E. Johnson, T. W. Hill, D. H. Pontius, W. S. Kurth, F. J. Crary, D. T. Young, M. F. Thomsen, D. B. Reisenfeld, A. J. Coates, G. R. Lewis, E. C. Sittler, and D. A. Gurnett (2006), The Interaction of the Atmosphere of Enceladus with Saturn's Plasma, Science, 311, 1409–1412, doi:10.1126/science.1121061.

Vasyliunas, V. M. (1983), Plasma distribution and flow, pp. 395–453.

Vogt, M. F., Kivelson, M. G., Khurana, K. K., Joy, S. P., and Walker, R. J. (2010), Reconnection and flows in the Jovian magnetotail as inferred from magnetometer observations, *J. Geophys. Res.*, 115, A06219, doi:10.1029/2009JA015098.

Vogt, M. F., Jackman, C. M., Slavin, J. A., Bunce, E. J., Cowley, S. W. H., Kivelson, M. G., and Khurana, K. K. (2014), Structure and statistical properties of plasmoids in Jupiter's magnetotail, *J. Geophys. Res. Space Physics*, 119, 821– 843, doi:10.1002/2013JA019393.

Went, D. R., Kivelson, M. G., Achilleos, N., Arridge, C. S., & Dougherty, M. K. (2011). Outer magnetospheric structure: Jupiter and Saturn compared. *Journal of Geophysical Research*, **116**, A04224. https://doi.org/10.1029/2010JA016045

Whipple, E. C. (1981), Potentials of surfaces in space, Reports on Progress in Physics, 44, 1197–1250, doi:10.1088/0034-4885/44/11/002.

Wilson, R. J., Bagenal, F., Delamere, P. A., Desroche, M., Fleshman, B. L., and Dols, V. (2013), Evidence from radial velocity measurements of a global electric field in Saturn's inner magnetosphere, *J. Geophys. Res. Space Physics*, 118, 2122–2132, doi:10.1002/jgra.50251.

Wing, S., P. T. Newell, and C.-I. Meng (2005), Cusp Modeling and Obser- vations at Low Altitude, Surveys in Geophysics, 26, 341–367, doi:10.1007/ s10712-005-1886-0.

Young, D. T., et al. (2004), Cassini Plasma Spectrometer investigation, *Space Sci. Rev.*, **114**, 1– 112, doi:10.1007/s11214-004-1406-4.

Zhong, J., et al. (2013), Three- dimensional magnetic flux rope structure formed by multiple sequential X- line reconnection at the magnetopause, *J. Geophys. Res. Space Physics*, **118**, 1904– 1911, doi:10.1002/jgra.50281.

Zhou, X.- W., and Russell, C. T. (1997), The location of the high- latitude polar cusp and the shape of the surrounding magnetopause, *J. Geophys. Res.*, 102(A1), 105– 110, doi:10.1029/96JA02702.

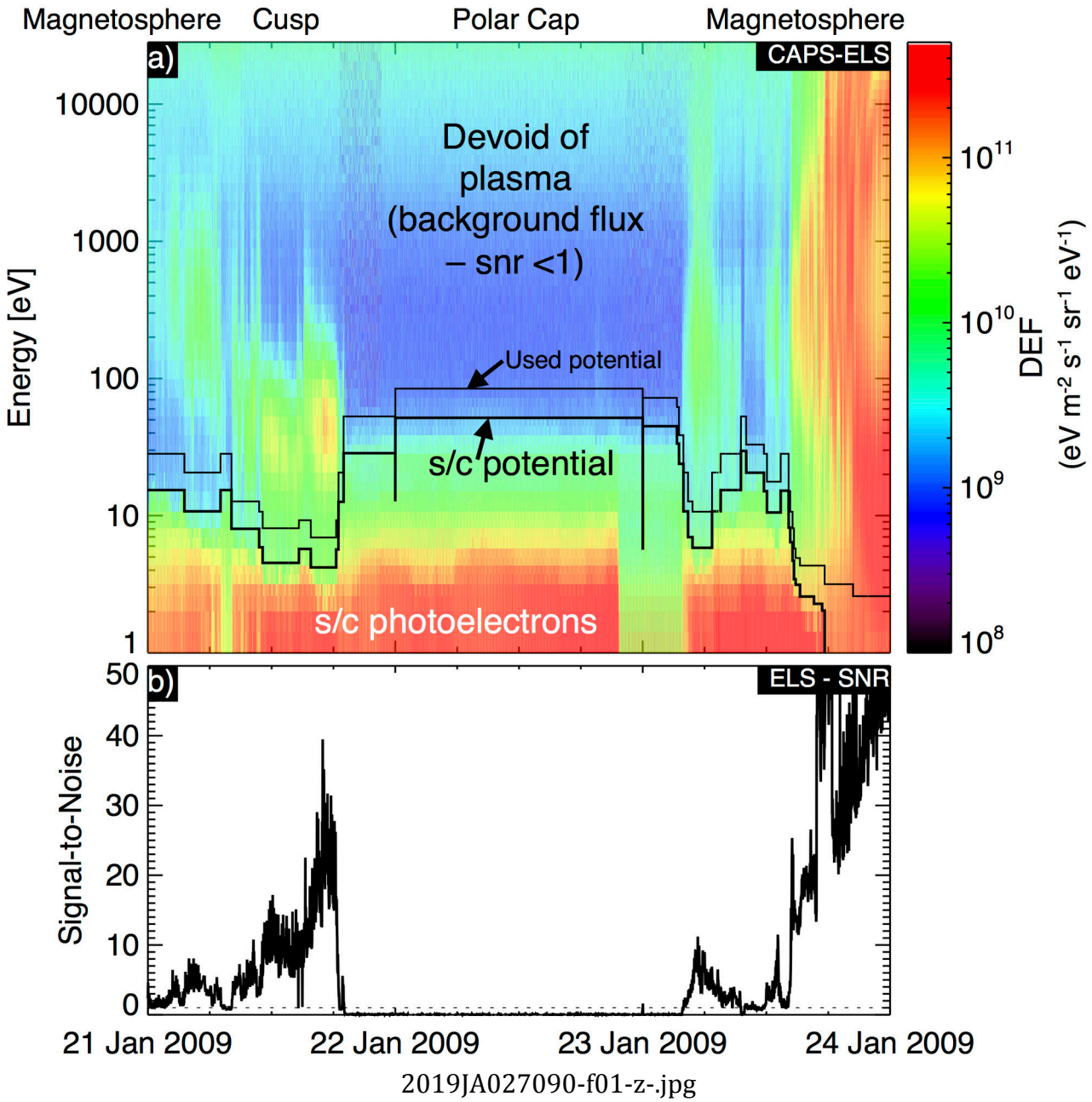

2019JA027090-f01-z-.jpg

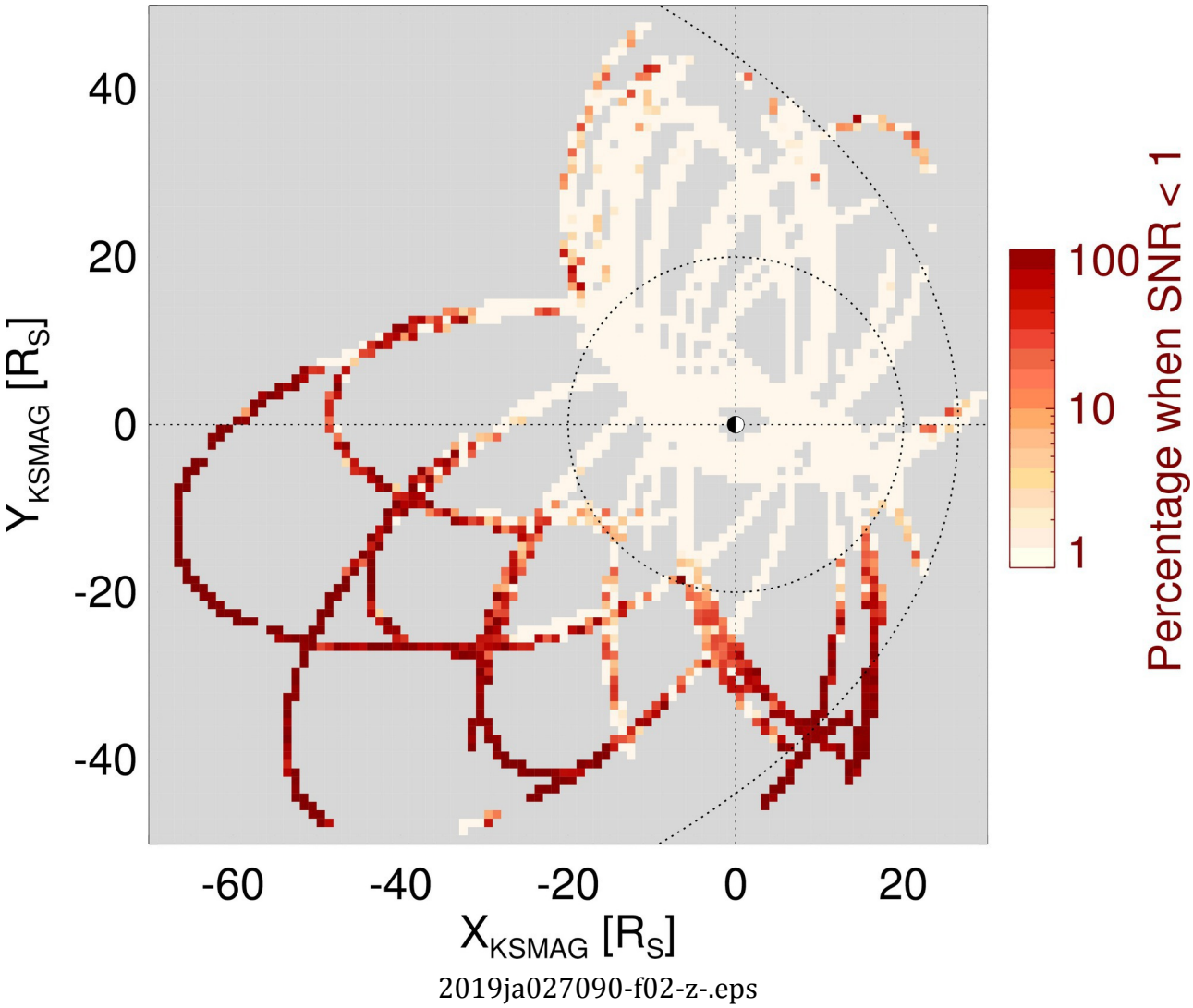

2019ja027090-f02-z-.eps

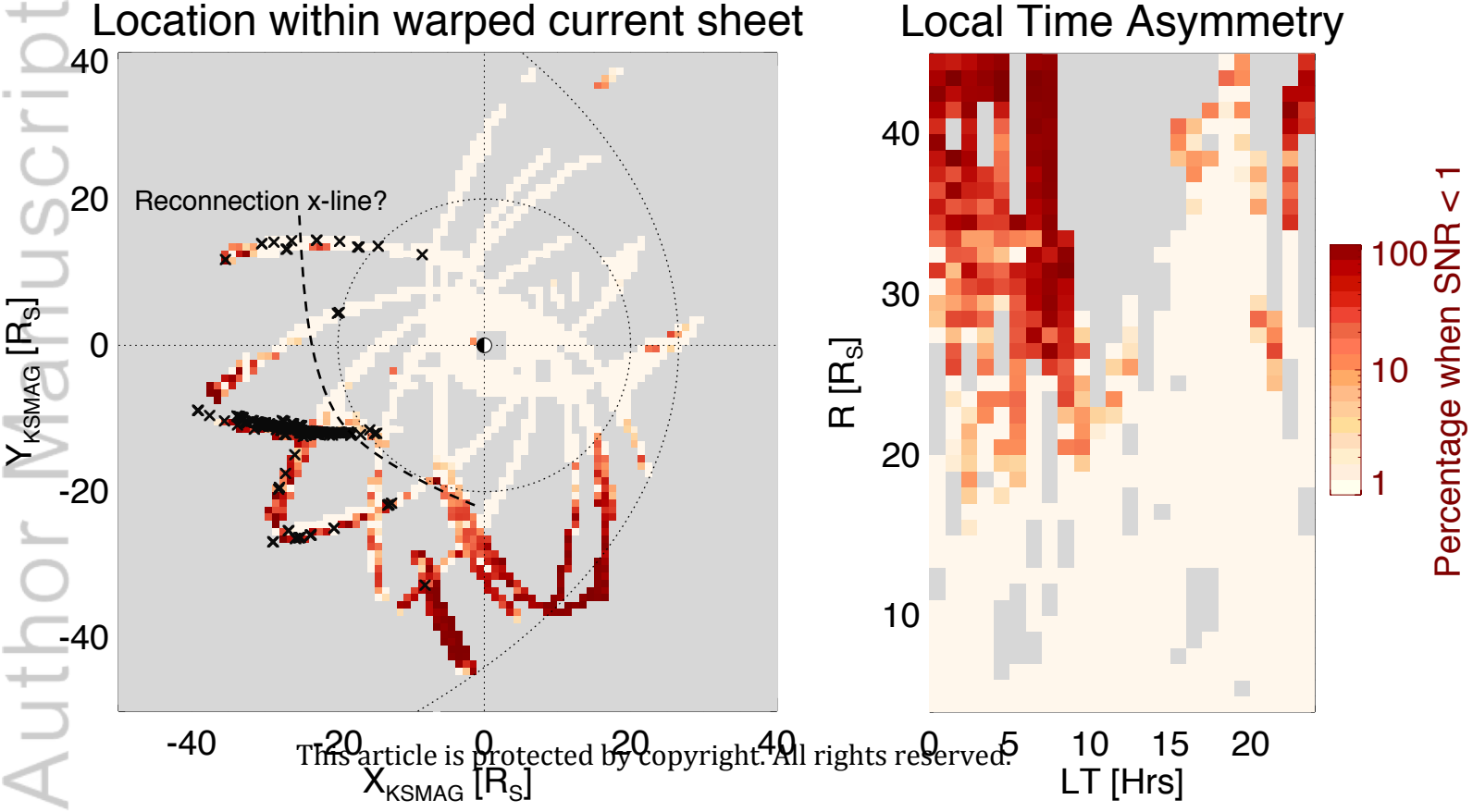

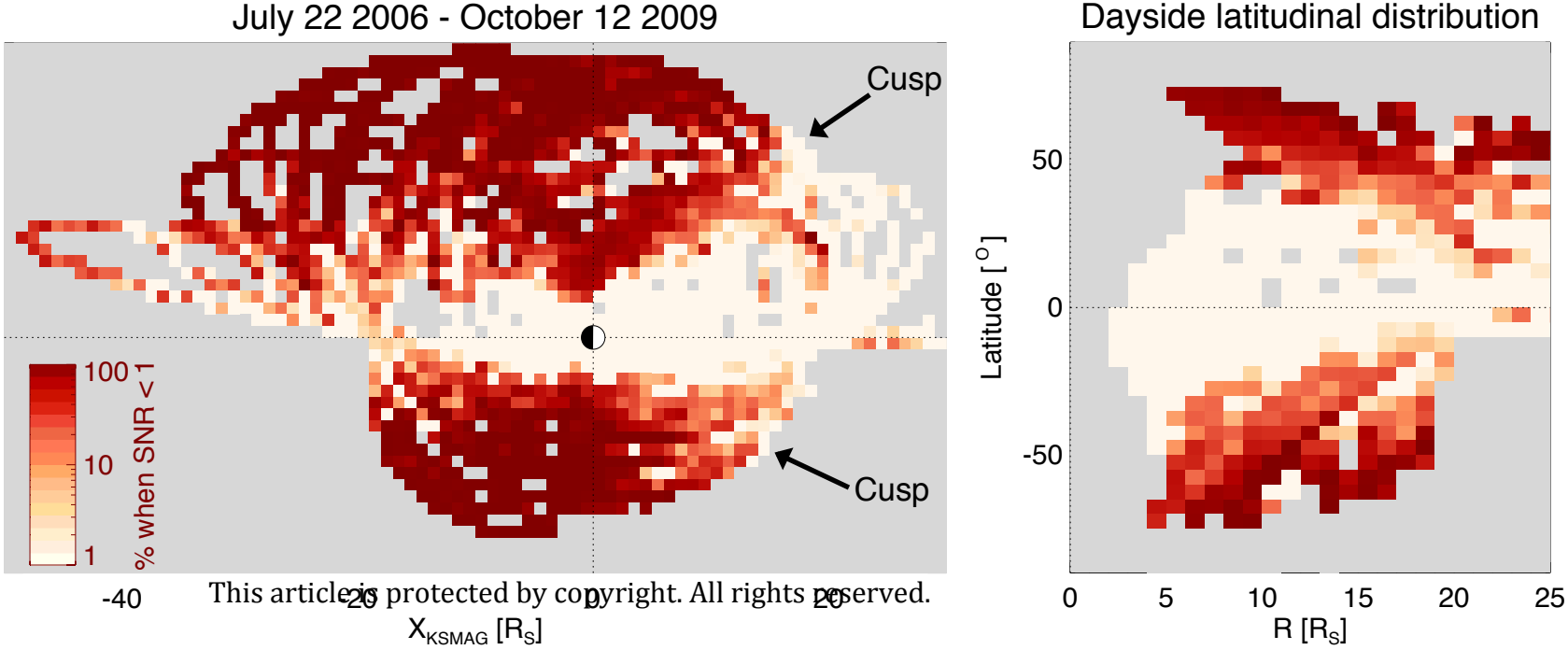

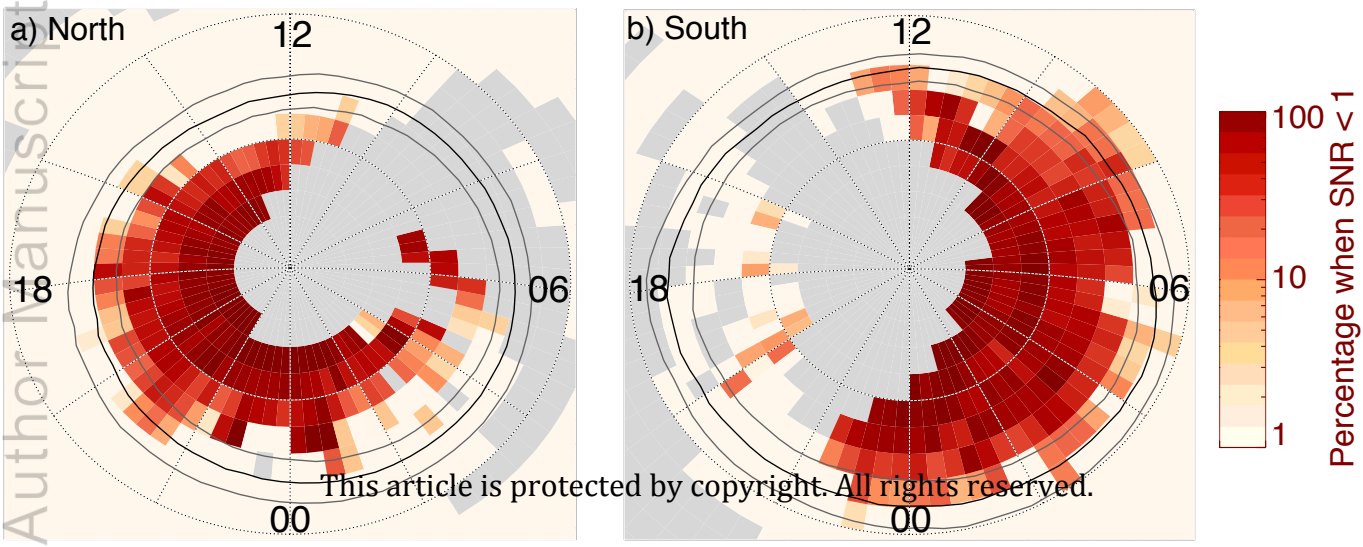

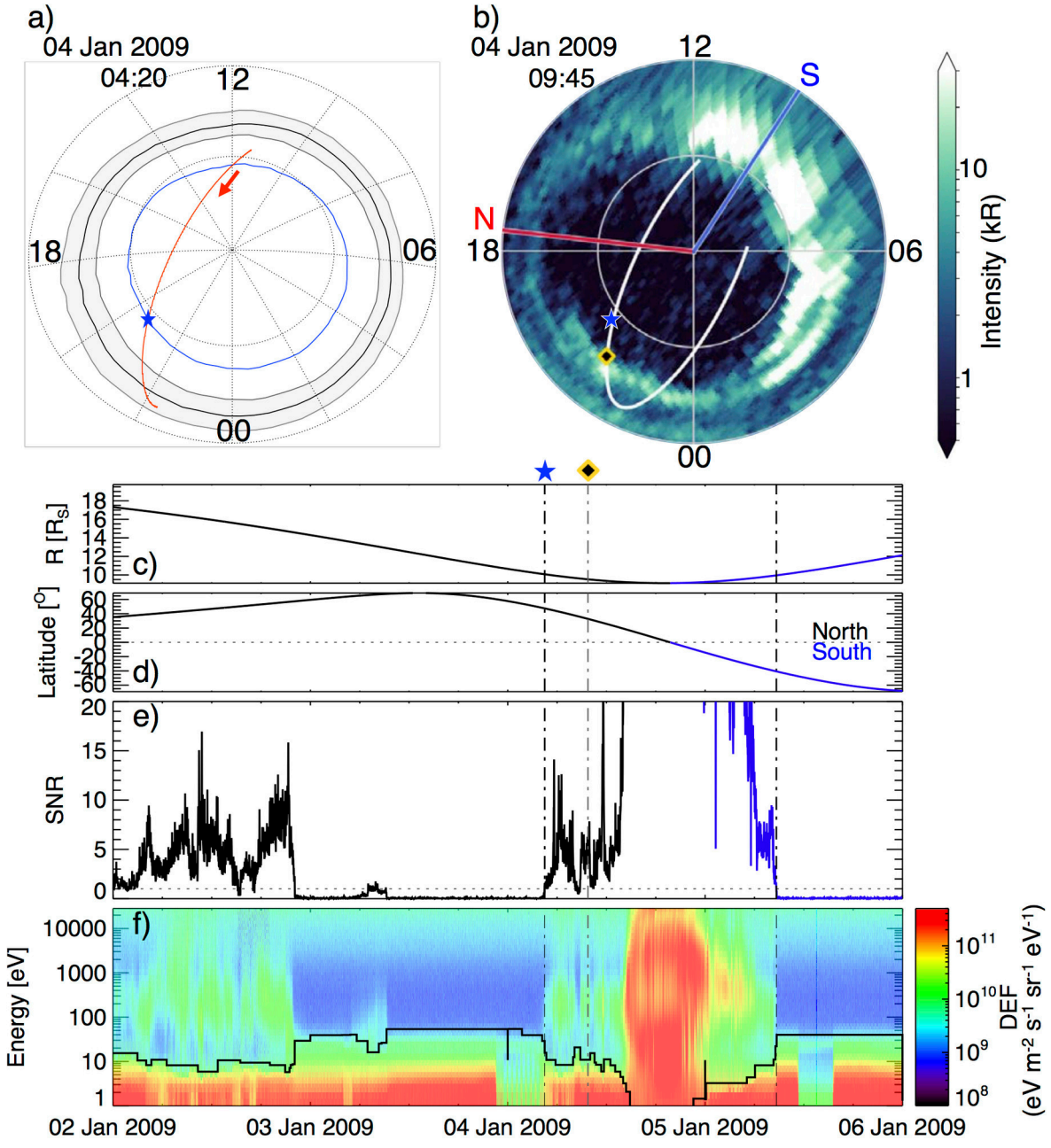

2019JA027090-f06-z-.jpg